



HHS Public Access

Author manuscript

Biomaterials. Author manuscript; available in PMC 2022 August 01.

Published in final edited form as:

Biomaterials. 2021 August ; 275: 120922. doi:10.1016/j.biomaterials.2021.120922.

Engineering a 3D Collective Cancer Invasion Model with Control over Collagen Fiber Alignment

Chia-Yi Su¹, Alice Burchett², Matthew Dunworth⁴, Jong Seob Choi¹, Andrew J. Ewald^{1,4,5}, Eun Hyun Ahn¹, Deok-Ho Kim^{1,3,*}

¹Department of Biomedical Engineering, Johns Hopkins University School of Medicine, Baltimore, MD, United States

²Department of Bioengineering, University of Washington, Seattle, WA, United States

³Department of Medicine, Johns Hopkins University School of Medicine, Baltimore, MD, United States

⁴Department of Oncology, Sidney Kimmel Comprehensive Cancer Center, Johns Hopkins University School of Medicine, Baltimore, MD, United States

⁵Department of Cell Biology and Center for Cell Dynamics, Johns Hopkins University School of Medicine, Baltimore, MD, United States

Abstract

Prior to cancer cell invasion, the structure of the extracellular matrix (ECM) surrounding the tumor is remodeled, such that circumferentially oriented matrix fibers become radially aligned. This predisposed radially aligned matrix structure serves as a critical regulator of cancer invasion. However, a biomimetic 3D model that recapitulates a tumor's behavioral response to these ECM structures is not yet available. In this study, we have developed a phase-specific, force-guided method to establish a 3D dual topographical tumor model in which each tumor spheroid/organoid is surrounded by radially aligned collagen I fibers on one side and circumferentially oriented fibers on the opposite side. A coaxial rotating cylinder system was employed to construct the dual

***Corresponding Author:** Professor Deok-Ho Kim, PhD, Department of Biomedical Engineering, The Johns Hopkins University School of Medicine, Office 724B, Ross Research Building, 720 Rutland Avenue, Baltimore, MD 21205, USA, Tel: 410-502-9773, dhkim@jhu.edu.

CRediT authorship contribution statement

Chia-Yi Su: Conceptualization, Methodology, Formal analysis, Validation, Investigation, Visualization, Writing - Original Draft; **Alice Burchett:** Methodology, Formal analysis, Validation; **Jong Seob Choi:** Investigation; **Matthew Dunworth:** Investigation; **Andrew J. Ewald:** Methodology, Writing - Review & Editing, Funding acquisition; **Eun Hyun Ahn:** Supervision, Visualization, Writing - Review & Editing, Funding acquisition; **Deok-Ho Kim:** Supervision, Writing - Review & Editing, Project administration, Funding acquisition

Publisher's Disclaimer: This is a PDF file of an unedited manuscript that has been accepted for publication. As a service to our customers we are providing this early version of the manuscript. The manuscript will undergo copyediting, typesetting, and review of the resulting proof before it is published in its final form. Please note that during the production process errors may be discovered which could affect the content, and all legal disclaimers that apply to the journal pertain.

Declaration of interest

DHK is a co-founder and scientific advisory board member at Curi Bio, Inc. AJE has unlicensed patents related to the use of keratin-14 as a biomarker in breast cancer and to the use of antibodies as cancer treatments. AJE's spouse is an employee of Immunocore.

Declaration of interests

The authors declare that they have no known competing financial interests or personal relationships that could have appeared to influence the work reported in this paper.

fiber topography and to pre-seed tumor spheroids/organoids within a single device. This system enables the application of different force mechanisms in the nucleation and elongation phases of collagen fiber polymerization to guide fiber alignment. In the nucleation phase, fiber alignment is significantly enhanced by a horizontal laminar Couette flow driven by the inner cylinder rotation. In the elongation phase, fiber growth is guided by a vertical gravitational force to form a large collagen matrix gel (35 x 25 x 0.5 mm) embedded with >1,000 tumor spheroids. The fibers above each tumor spheroid are radially aligned along the direction of gravitational force in contrast to the circumferentially oriented fibers beneath each tumor spheroid/organoid, where the presence of the tumor interferes with the gravity-induced fiber alignment. After ten days of invasion, there are more disseminated multicellular clusters on the radially aligned side, compared to the side of the tumor spheroid/organoid facing circumferentially oriented fibers. These results indicate that our 3D dual topographical model recapitulates the preference of tumors to invade and disseminate along radially aligned fibers. We anticipate that this 3D dual topographical model will have broad utility to those studying collective tumor invasion and that it has the potential to identify cancer invasion-targeted therapeutic agents.

Keywords

extracellular matrix; aligned collagen fibers; tumor dissemination; collective cell invasion; tumor organoids; Couette flow

1. Introduction

Cancer progression is a dynamic process of tumor cells interacting with their microenvironment [1]. Cancer cells interact with tumor stromal cells to continuously remodel their microenvironment even before local invasion [2, 3] and distant metastasis [4, 5]. In turn, the remodeled tumor microenvironment distinguishes itself from normal tissue by providing biophysical and biochemical cues as a route of cancer invasion [6, 7]. Together, the reciprocal interaction between cells and extracellular matrix (ECM) forms a synergistic loop to drive tumor progression. Structural remodeling of the ECM surrounding tumors is one consequence of cell-ECM interaction [8]. Invading cancer cells align surrounding ECM fibers to form a “migration highway,” which guides tumor cells to efficiently penetrate through stroma [9–11]. Furthermore, the predisposed tumor ECM structure at the tumor border can be formed even before cancer invasion. For example, the alteration of the stromal microenvironment is a major factor driving the progression from preinvasive breast cancer, ductal carcinoma *in situ* (DCIS), to invasive ductal carcinoma (IDC). In contrast, there are only modest genetic changes between cancer cells in IDC and DCIS [2, 12]. In DCIS patients, the predisposed radially oriented matrix structure predicts poor prognosis [13]. Direct evidence from experimental mouse models reveals that radially aligned fibrillar collagen structure promotes breast tumor invasion [14, 15]. Also, an *in vitro* tumor model demonstrates that tumor spheroids can remotely orient collagen fibers up to a distance of five times the spheroid radius from the spheroid border [16].

Regarding the ECM-to-cell effect, previous studies indicated that aligned fiber topography guides tumor cell movement by enhancing migration persistence and velocity [9, 17].

However, most studies focused on responses of individual cells to aligned topography, and little is known about how tumor spheroids or organoids react to predisposed ECM structure, mainly due to the lack of relevant experimental models [18–21]. Unlike matrices containing scattered individual cells, tumor spheroid models better recapitulate *in vivo* collective cell migration, tumor invasion, and metastasis [22]. However, elucidating how tumor spheroids/organoids respond to various ECM structures requires more complicated bioengineering approaches. A major obstacle in engineering a 3D topographical tumor spheroid/organoid model is to encompass multicellular tumor spheroids with specialized ECM architecture without damaging ECM structure.

Previous studies created aligned collagen fibers by applying different methods such as extensional strain [23–25], electrospinning [26–28], magnetic field [29, 30], microfluidics [31–33], and cell remodeling [18, 19, 34]. Among all the existing methods to align ECM fibers, cell remodeling [18, 19, 34] and microfluidics [20, 21, 25] are the most commonly used to build tumor models with a predisposed ECM structure (Table 1). However, common limitations of these methods are that fiber alignment is confined to a small or restricted area [20, 34] and difficulties with embedding tumor spheroids in the matrix. Thus, embedding or attaching tumor spheroids to the matrix after the formation of fiber alignment risks interrupting the preformed ECM structure [18, 19, 34]. Microfluidic methods may only be suitable for single-cell models and are difficult to apply to tumor spheroid models because the pre-seeded tumor spheroids interfere with the flow that drives fiber alignment. In addition, it is difficult to embed tumor spheroids in electrospun scaffolds due to their low porosity [35]. Therefore, despite their utility for studying individual cell invasion, currently available models of aligning matrix fibers are not applicable to study collective cell invasion of tumor spheroids/organoids. A novel model that enables us to seed tumor spheroids/organoids and control fiber pre-alignment is needed to investigate collective cancer cell invasion.

To develop a 3D topographical tumor spheroid/organoid model, we established a novel method to efficiently create a large-scale collagen gel with tumor spheroids/organoids surrounded by dual ECM topography. We applied a phase-specific, force-guided method for collagen polymerization. [32, 36]. In the nucleation phase, the first phase of collagen polymerization, a horizontal laminar Couette flow was generated by rotating the inner cylinder in a coaxial rotating cylinder system to promote the adsorption of collagen monomers onto the surface and form an initial coating of collagen. Next, in the elongation phase, a vertical gravitational force was adopted to guide the direction of collagen fibril assembly. This new topography system presents several advantages. First, a higher fiber alignment is achieved than applying the gravitational force alone. Second, unlike most microfluidics, our coaxial rotating cylinders enable the seeding of tumor spheroids. Third, each tumor spheroid is surrounded on one half by radially aligned fibers and the other half by circumferentially oriented fibers. Since the individual tumor spheroids are interacting simultaneously with the two most common topographical features of tumor stroma, our model is ideal for studying how 3D topography affects tumor invasion. Our results indicate that radially aligned topography promotes tumor invasion by enhancing cluster-based dissemination of tumor cells. Disseminated multicellular clusters budding out from the main tumor on radially aligned collagen fibers in our 3D model authentically recapitulates human

cancer invasion. We anticipate that our 3D topographical tumor model can be readily applied to investigate collective invasion across cancer types and to identify new cancer therapies.

2. Materials and Methods

2.1. Design and assembly of the coaxial rotating cylinder system

Our coaxial rotating cylinder system comprises two borosilicate glass scintillation vials (Sigma-Aldrich, USA) with different radii that were concentrically aligned by a customized 3D printed base, a brass rod, and plastic bearings. The outer cylinder is held fixed by the base, while the inner cylinder is free to rotate about its axis. The portion above the neck of the outer glass vial was cut off by a glass cutter for the inner glass vial to fit in. The rotation of the inner glass cylinder was powered by a direct current 6 volt 500 revolutions per minute (rpm) micro speed reduction motor, and the rotation speed was controlled by a pulse-width modulation stepless direct current motor speed controller. The brass rod attached to the inner glass cylinder was connected to the motor shaft by a customized 3D-printed part. The 3D printed base and parts were designed using Autodesk Inventor software (Autodesk, USA) and printed by a desktop 3D printer (Cubicon, Korea) with acrylonitrile butadiene styrene filaments. After being concentrically aligned, the smaller inner glass cylinder was placed inside the center of the larger outer glass cylinder leaving an empty annulus between the two cylinders for collagen gelling.

2.2. Fabrication of collagen matrices with aligned fibers

Collagen matrices were prepared by mixing type I rat tail telocollagen solution and neutralization solution in a ratio of 9:1 at a final concentration of 3.69 mg/ml (lot. 8282, RatCol® Rat Tail Collagen for 3D Hydrogels, Advanced BioMatrix, USA). Type I collagen solution was kept on ice before mixing. After mixing 900 μ L of type I collagen solution with 100 μ L neutralization buffer, a 1 mL collagen pregel solution was poured into the space between the two glass cylinders, and the inner cylinder was immediately rotated. A 2-minute rotation of the inner cylinder at 50 rpm was applied to generate Couette flow for collagen monomer nucleation on the glass surface and followed by a 20-minute gelling in a stationary condition for the gravitational force to guide collagen fiber elongation. Collagen was polymerized at room temperature.

2.3. Computational fluid dynamic simulation

A computational fluid dynamic simulation was performed using COMSOL Multiphysics version 5.5 (COMSOL, USA). First, a 2D geometry of a rectangle with the cross-section dimensions of the space between two glass cylinders was built. The density and dynamic viscosity of the collagen solution were input as material properties. Then, to simulate the fluid dynamics with the inner cylinder rotating, the inner wall of the 2D rectangle was set as a sliding wall, and the center axis of both cylinders was fixed as the symmetry. Laminar flow was applied as the physical model, and the fluid flow was described following Navier-Stokes equations [37]. Finally, the parameter sweep was set under various rotation speeds of the inner cylinder to determine the ideal shear rate for collagen nucleation.

2.4. Alignment and orientation analysis of collagen fibers

The collagen fibers in gels were visualized by an Olympus FV1000 multiphoton second-harmonic generation (SHG) microscope (Olympus, Japan) or a multiphoton second-harmonic generation (SHG) and confocal microscope (Zeiss LSM 710NLO-Meta, Germany). Images of 20 randomly picked locations were taken for each collagen gel. The SHG microscopic images were segmented and analyzed computationally by CT-FIRE, a MATLAB-based program, to quantify the orientation of collagen fibers [38]. To compare the alignment and orientation between experimental conditions, we performed directional statistics analysis using CircStat, a MATLAB program for circular statistics [39].

The fiber alignment was determined by resultant vector length from 20 random images for each gel. The value of resultant vector length ranges between 0 and 1. When the value is closer to 1, the fiber orientation angle is more concentrated around the mean direction, indicating more aligned fibers.

$$\text{Resultant vector length} = \sqrt{\left(\frac{1}{N} \sum_{i=1}^N \cos\theta_i\right)^2 + \left(\frac{1}{N} \sum_{i=1}^N \sin\theta_i\right)^2}$$

An alignment index representing the peakedness was introduced as a second method to assess the fiber alignment. The alignment index is equal to the highest frequency percentage (h) of angular distribution divided by the half of full width at a half maximum (FWHM) [24]. A value of 0 represents random distribution. The higher the value is, the more aligned the fibers are.

$$\text{Alignment index} = \frac{h}{\text{FWHM} \times 1/2}$$

The fiber orientation was represented by mean resultant vector. The mean resultant vector between experimental conditions was tested by the Watson-Williams test [39].

$$\text{Mean resultant vector} = \frac{1}{N} \sum_{i=1}^N \begin{pmatrix} \cos\theta_i \\ \sin\theta_i \end{pmatrix}$$

2.5. Scanning electron microscopy (SEM)

Images of the fibrous collagen morphology were taken using SEM (Apreo, Thermo Fisher Scientific, USA). The collagen gel samples were lyophilized at -80°C and high-vacuum status (0.07 millibar) via a Freeze Dry System (FreeZone Plus 2.5 Liter Cascade Benchtop Freeze Dry System, Labconco, USA). The lyophilized samples were coated with Au/Pt by a sputter coater for 60 seconds. Next, the samples were placed into the SEM vacuum chamber, and a 5kV of accelerating voltage was applied to acquire high-resolution images.

2.6. Cell culture

MCF7, T47D, and MDAMB231 human breast cancer cells were purchased from American Type Culture Collection (VA, USA). MCF7 and MDAMB231 cells were maintained in Dulbecco's Modified Eagle's Medium (DMEM) (Gibco, USA), and T47D cells were maintained in RPMI 1640 medium (Gibco, USA). Media were supplemented with 10% fetal bovine serum (Thermo Fisher Scientific, USA) and 1% penicillin-streptomycin (10,000 U/mL) (Thermo Fisher Scientific, USA). The cells were incubated under a 5% CO₂ humidified atmosphere at 37 °C.

2.7. Development of dual topographical tumor spheroid and organoid model

Tumor spheroids were generated using AggreWell 400 6-well microwell culture plates (STEMCELL Technologies, USA) [40]. Before seeding cells in microwell culture plates, 0.5 mL anti-adherence rinsing solution (STEMCELL Technologies, USA) was added into each well, and a 2-minute 2000 g centrifugation followed by a 30-minute incubation at 37 °C was performed to prevent cell adhesion onto the microwells. Next, a 2.5 million single-cell suspension in 2 mL was seeded in each well. A 5-minute 200 g centrifugation was performed to cluster the cells in microwells, and the cells were incubated in a CO₂ incubator at 37°C overnight for cells to aggregate and form spheroids. Tumor spheroids generated from a well of a 6-well microwell culture plate were harvested, and one-fourth of the tumor spheroids in 100 µL medium were mixed and seeded together within a 1 mL collagen pregel solution (900 µL of type I collagen solution and 100 µL neutralization buffer) at a final concentration of 3.35 mg/ml (lot. 8282, RatCol® Rat Tail Collagen for 3D Hydrogels, Advanced BioMatrix, USA), and poured into the space between the two coaxial cylinders.

Mouse mammary tumor organoids were derived from two genetically engineered mouse models of breast cancer, MMTV-PyMT [41] and C3(1)-Tag [42], as described previously [43]. Mammary tumors harvested from MMTV-PyMT or C3(1)-Tag mice were mechanically minced and enzymatically digested by collagenase and trypsin. Single cancer cells or stromal cells were separated from epithelial tumor organoids by a series of differential centrifugation. Around 1500 mammary tumor organoids in 100 µL of medium were mixed with a 1 mL collagen pregel solution and seeded together into the space between the two coaxial cylinders. All mice were female and were obtained from The Jackson Laboratory (Bar Harbor, ME). All procedures were conducted by following protocols approved by the Johns Hopkins Medical Institute Animal Care and Use Committee (IACUC).

For the Couette + gravity group, collagen fibers were polymerized in the coaxial cylinder system under a 2-minute laminar Couette flow driven by inner cylinder rotation at 50 rpm followed by a 20-minute gravity-driven fiber elongation. For the gravity only group, collagen fibers were polymerized in the coaxial cylinder system with a 20-minute gelling in a stationary condition. Collagen was polymerized at room temperature. The resulting tube-shaped collagen gels embedded with tumor spheroids/organoids were then cut and spread out to form dual topographical tumor models. MCF7 and MDAMB231 tumor spheroids were maintained in DMEM medium (Gibco, USA), and T47D tumor spheroids were

maintained in RPMI 1640 medium (Gibco, USA). Media were supplemented with 10% fetal bovine serum (Thermo Fisher Scientific, USA) and 1% penicillin-streptomycin (Thermo Fisher Scientific, USA). MMTV-PyMT and C3(1)-Tag tumor organoids were maintained in DMEM-F12 medium (Gibco, USA) supplemented with 1% insulin–transferrin–selenium (Gibco, USA), 1% penicillin-streptomycin (Sigma, USA), and 2.4 nM FGF2 (Sigma, USA).

2.8. Cancer invasion pattern analysis

After a 10-day culture in collagen gels, tumor spheroids were stained with CellTracker Red CMTPX Dye (Thermo Fisher Scientific, USA) and Hoechst 33342 (Thermo Fisher Scientific, USA) and fixed with 4% paraformaldehyde (Thermo Fisher Scientific, USA). A spinning disk confocal microscope (Nikon TiE inverted widefield microscope and Yokogawa W1 spinning disk, Japan) or a multiphoton second-harmonic generation (SHG) and confocal microscope (Zeiss LSM 710NLO-Meta, Germany) was used to image tumor spheroids. Images were analyzed by a customized macro in ImageJ. In brief, Z stack confocal images of a whole tumor spheroid/organoid were processed by Background Subtraction, Z projection, and Make Binary. The area, perimeter, orientation angle, and other parameters of binary images were quantified with the Analyze Particles function. Disseminated cell clusters were defined as cells with no continuous connection with the main tumor in binary images. The morphology complexity of tumor spheroids was presented by border complexity [44].

$$\text{Border complexity} = \frac{(\sum \text{perimeter})^2}{4\pi \times \sum \text{area}}$$

The higher the border complexity, the more irregular the tumor. When invasion occurs, the invasion projection increases the border complexity by a greater border perimeter for a corresponding area. When disseminated cell clusters appear, the perimeter and area of both the main spheroid and disseminated cell clusters were taken into calculation. To compare the border complexity between radial and circumferential zone in the same tumor spheroids/organoids, we divided the binary image of a whole tumor spheroid/organoid into two images using the widest short axis of the spheroid/organoid as the separating line.

2.9. Statistical analysis

Data were analyzed using GraphPad Prism 9 (GraphPad Software, USA). The frequency distributions collagen fiber orientation was compared by Kolmogorov-Smirnov test. Fiber alignment (resultant vector length) between experimental conditions was compared by one-way ANOVA. The border complexity of tumor spheroids/organoids and the number and size of disseminated cell clusters between experimental groups were compared by one-way ANOVA. Spheroid morphology in different ECM structures was compared using the Student's t-test, one-way ANOVA, or Wilcoxon matched-pairs signed-rank test. For directional statistics, the alignment and orientation parameters of collagen fibers were analyzed on a MATLAB program, CircStat [39]. The mean resultant vectors between samples were compared by the Watson-Williams test. For all statistical analyses, the difference was considered significant at $p < 0.05$.

3. Results

3.1. Collagen fibers are aligned using a phase-specific, force-guided method

A proof of concept to develop a phase-specific, force-guided method for aligning collagen fibers in a 3D matrix gel is based on the two-phase nature of collagen fiber polymerization, with nucleation and elongation phases [32, 36]. Type I collagen was used to create the 3D matrix for modeling breast cancer invasion because it is one of the most abundant ECM components in breast tumors and plays a critical role in tumor progression [45, 46]. Figure 1A shows the working principle and fabrication process of our method to create a large collagen gel with aligned fibers. During the nucleation phase, we applied a horizontal laminar Couette flow to deposit collagen monomers on the cylinder glass surface. This increases the initial collagen monomer coating, which forms a collagen mat on the glass substrate, improving the collagen fiber formation and alignment [32]. The nucleation of collagen occurred within the first two minutes of polymerization [32]. Therefore, the inner cylinder was set to rotate for the first 2 minutes to adsorb a collagen monomer mat onto the surface to form an initial coating of collagen. Then, after inner cylinder rotation was stopped, the force orientation was changed to vertical gravitational force to guide collagen fibers to grow vertically in the elongation phase [31, 32].

3.2. A coaxial rotating cylinder system is applied to align collagen fibers in a 3D matrix

To develop a device that accommodates forces for both the nucleation and elongation phases, we applied a coaxial rotating cylinder instead of microfluidics for the following reasons (Figure 1A). First, as a closed system, the shear force driven by laminar Couette flow can be easily controlled by tuning the rotation speed of the cylinder without external equipment such as a syringe pump. Since the nucleation phase occurs quickly within two minutes [32], our system does not need a syringe pump to drive the flow, thereby shortening the preparation time and reducing the probability of nucleation occurring outside of the system. Second, stopping the inner cylinder rotation immediately shifted the laminar shear flow to the vertical gravitational force to allow collagen fiber elongation. Third, our method creates a large collagen gel with homogeneously aligned fibers compared to the limited space in microfluidics. Fourth, our coaxial rotating cylinders system is a stable environment to seed spheroids/organoids inside collagen during polymerization [47].

We designed our coaxial rotating cylinder system to create a laminar Couette flow upon rotation of the inner cylinder. We used a larger borosilicate glass scintillation vial (radius of 13.7 mm) as the outer cylinder and a smaller borosilicate glass scintillation vial (radius of 11.4 mm) as the inner cylinder (Figure 1B). The radius ratio of the two concentric cylinders was 0.83, which is > 0.8 , the criteria to form laminar Couette flow [47]. To coaxially align the inner and outer cylinders, we designed and 3D-printed a pyramid-shaped base, together with a brass rod and plastic bearings to hold the inner cylinder in the middle of the outer cylinder. (Figure 1C). The resulting open-topped annulus between the inner and outer cylinders allowed space to pour the mixture of collagen solution and neutralization buffer. Then, the laminar Couette flow driven by the rotating inner cylinder initiated the coating of collagen monomers on the cylinder glass surface. The rotation speed ranging from 0 to 500 rpm was stably regulated by a motor and stepless motor speed controller (Figure 1D).

To determine an optimum rotation speed for collagen nucleation and validate our device design to create a laminar Couette flow, we performed a computational fluid dynamics simulation on COMSOL Multiphysics. The simulation results with a rotating inner cylinder showed laminar Couette flow without turbulent Taylor vortices at 50 rpm rotation and up to 500 rpm, the highest rotation speed limit of the motor (Figure 2A and 2B). Our finding was consistent with previous studies showing a stable laminar flow without turbulence at a low rotation speed [48]. On glass substrates, an intermediate shear rate between 20 to 80 s^{-1} has been demonstrated to best align collagen fibers (3 mg/ml) compared to a lower shear rate of 9 s^{-1} or a higher shear rate of 500 s^{-1} [32]. Based on our simulation results of shear rate at different rotational speeds, we determined the inner cylinder rotation speed at 50 rpm to achieve the desired shear rate of 35 s^{-1} (Figure 2C) and flow velocity of 0.03 m/s (Figure 2D) on the surface of the inner cylinder. We measured the desired rotation speed using shear rate, rather than shear force, for the following reasons: shear rate does not change as concentration or viscosity changes, and shear rate independently increases collagen nucleation by excluding flow rate as a confounding factor [32].

Couette flow was stopped before any gross gel solidification could be observed. After the 2-minute rotation period, the collagen began its elongation phase under the influence of vertical gravitational force. During this elongation phase, collagen fibers grew along vertical gravitational force after stopping the 2-minute rotation of the inner cylinder. No bulk movement of the gel was seen during the rotation- or gravity-driven phase. An intact tube-shaped gel was formed after a 2-minute rotation and an additional 20-minute gelling period in a stationary condition (Figure 1E). In contrast, a 10-minute or a 5-minute rotation did not form an intact gel. Instead, fragmented collagen debris was formed even after a 60-minute gelling in a stationary condition (Supplementary Figure 1A). After generating an intact tube-shaped gel, we cut and spread the gel to make a large rectangular collagen matrix gel (35 mm x 25 mm x 0.5 mm) (Figure 1E). Gravity only and a random condition were used as control groups. In the gravity only group, collagen was polymerized in the coaxial cylinder system in a stationary condition without the initial 2-minute rotation. In the random group, collagen pregel solution was poured onto a glass slide with a polydimethylsiloxane (PDMS) frame designed to have the same dimension as the space between two cylinders in the coaxial cylinder system (Supplementary Figure 1B). The collagen matrices were gelled on glass slides in a stationary condition to form randomly oriented collagen fibers.

3.3. Collagen fiber alignment is enhanced by laminar Couette flow followed by gravitational force

Collagen fibers in 3D matrix gels formed under different experimental conditions were visualized by a multiphoton SHG microscope (Figure 3A) and computationally segmented using CT-FIRE, a MATLAB-based program (Figure 3B). We compared the alignment and orientation of collagen fibers in the 3D matrix gel formed in different experimental conditions. First, we analyzed the directional statistics of collagen fibers in 20 randomly picked spots from one gel for each experimental condition. The angular frequency distribution analysis of collagen fibers demonstrated that resultant vector length was higher in the Couette + gravity group (0.8) than in the gravity only (0.7) or random (0.59) groups. (Figure 3C and 3D). The fiber orientation angles were also significantly different between

the 2-minute rotation group (79.34°) and the no rotation group (90.14°) (Figure 3C and 3D). These results suggested that the additional laminar Couette flow promoted fiber alignment and contributed to the fiber orientation deviation ($p < 0.0001$). In addition, SEM images confirmed more aligned but oblique collagen fibers in the Couette + gravity group compared to the gravity only group (Figure 3E). Our findings, along with previous studies, suggest the orientation of collagen fibers was the combined consequence of the flow direction in both nucleation and elongation phases [32].

To validate the reproducibility of our method, we performed three independent experiments and investigated the fiber alignment by determining the angular frequency distribution (Figure 3F) and resultant vector length (Figure 3G) of collagen fibers. The peak frequency distribution was higher in the Couette + gravity group (13.91% at 80°) than in the gravity only (8.33% at 90°) and random (7.59% at 170°) groups (Figure 3F). Resultant vector length analyses demonstrated that applying both Couette flow and gravity significantly enhanced fiber alignment in comparison to gravity only ($p < 0.01$) and random ($p < 0.001$) groups (Figure 3G). As a second measure of fiber alignment, alignment indexes derived from the frequency distribution were also significantly higher in the Couette + gravity group than in gravity only and random groups (Supplementary Figure 1C). The alignment and orientation analysis results demonstrated the reproducibility of our novel technology to generate a large collagen matrix gel with homogeneously aligned fibers.

3.4. Each tumor spheroid is surrounded by radially aligned and circumferentially oriented collagen fibers in dual topographical tumor model

We pre-seeded tumor spheroids within the collagen solution before gelling to allow the close contact of tumor spheroids with the *in vivo* tumor-like ECM topography. Tumor spheroids of MCF7 and T47D breast cancer cells were uniformly generated in a spherical shape in microwells (Figure 4A and Supplementary Figure 2A). Approximately 1500 tumor spheroids were suspended in 1 mL of collagen solution to achieve a density of two tumor spheroids per mm^3 . Then, the mixture of collagen solution and tumor spheroids in the coaxial cylinder system underwent 2 minutes of laminar Couette flow and 20 minutes of gravitational force to align collagen fibers (Figure 4A and Supplementary Figure 2B). Immediately after collagen gels were formed, we analyzed the collagen fiber orientation surrounding tumor spheroids using SHG microscopy. Interestingly, collagen fibers surrounding tumor spheroids exhibited a location-specific topography, in which collagen fibers above spheroids were radially aligned, and fibers beneath spheroids were circumferentially oriented (Figure 4B bottom and 4C). This location-specific dual topography was not observed in the collagen gel without tumor spheroids or in random groups with tumor spheroids (Figure 4B top and 4C), where collagen was gelled with spheroids on glass slides. In comparison, collagen fibers polymerized only by gravitational force without Couette flow exhibited weaker radial alignment above spheroids (Figure 4B middle, 4C, and 4D). Therefore, we concluded that Couette flow with subsequent gravitational force significantly enhanced fiber alignment in the radial zone above tumor spheroids.

To prove that this location-specific topography is not due to tumor cell contractility, we embedded 200 μm glass microbeads instead of tumor spheroids. We found the same location-specific topography where fibers above microbeads were radially aligned, and fibers beneath microbeads were circumferentially oriented. This result ruled out the possibility that the location-specific topography was due to tumor cell contractility (Supplementary Figure 2D and 2E). Furthermore, there was no difference in fiber density between the radial zone above spheroids and the circumferential zone beneath spheroids (Figure 4E), which suggests that the circumferentially oriented topography beneath tumor spheroids was more likely due to spheroids' interference with collagen fiber elongation, rather than aggregated fibers by spheroid weight. The interference of fiber orientation by objects during fiber elongation was reported in a previous study in which cylindrical microposts in a microfluidic device interfered with the fluid flow-guided fiber alignment [21]. No difference in fiber density, suggesting similar mechanical properties [49] between radial and circumferential zones, also suggests that matrix topography can serve as an independent factor in determining tumor invasion patterns. Finally, we verified that the 2-minute Couette flow did not affect the morphology and border complexity of tumor spheroids, indicating that the shear forces from Couette flow did not disrupt tumor spheroid integrity (Figure 4F and Supplementary Figure 2C). Our dual topographical tumor model enables spheroids to be in contact with two most common tumor ECM topographical structures, which recapitulates *in vivo* tumor microenvironment and makes this model applicable to investigate collective cancer invasion.

3.5. Radially aligned ECM topography promotes a cluster-based cancer invasion

Tumor invasion patterns were analyzed after a 10-day interaction of T47D and MCF7 tumor spheroids with the predisposed collagen fiber structure. Images of MCF7 tumor spheroids after a 10-day invasion in dual topographical model demonstrated evenly distributed tumor spheroids and the same invasion pattern toward radially aligned fibers (Figure 5A). SHG images of T47D cells demonstrated that the ECM topography on day 10 (Figure 5B) remained similar to the predisposed topography on day 0 (Figure 4B). Fibers in the radial zones retained radially aligned structure, and fibers at the circumferential zones were still circumferentially oriented. No prominent remodeling of predisposed collagen fiber structure was observed. Both SHG and confocal images revealed multicellular disseminated clusters and finger-like projections invading along radially aligned collagen fibers but not in circumferentially oriented fibers (Figure 5C and 5D; Supplementary Movie 1 and 2). In the fibers polymerized only by gravitational force without Couette flow, fewer multicellular disseminated clusters and finger-like projections were observed along the weakly aligned fibers (Figure 5C and 5D). Border complexity analysis confirmed that spheroids in Couette + gravity groups had a more irregular border compared to the gravity only and random groups ($p < 0.0001$ for both MCF7 and T47D) (Figure 5E and 5F). In random groups where breast cancer spheroids were surrounded entirely by circumferentially oriented collagen fibers, tumors formed ductules recapitulating well-differentiated human breast cancer (Supplementary Movie 3). In contrast, the disseminated multicellular clusters and projections observed at the tumor border along radially aligned fibers recapitulated the morphology of poorly differentiated breast cancer (Supplementary Movie 4).

We examined the intra-spheroid morphology responding to two distinct ECM structures, circumferentially orientated or radially aligned (Figure 6A). The orientation analysis indicated that multicellular clusters disseminated from tumor spheroids invaded and elongated along the collagen fiber direction (Figure 6B). The side of tumor spheroids interacting with radially aligned fibers had more disseminated cell clusters ($p < 0.001$ for MCF7 and $p < 0.01$ for T47D) (Figure 6C) and a more irregular border compared to the other side of tumor spheroids interacting with circumferentially oriented fibers ($p < 0.0001$ for both MCF7 and T47D) (Figure 6D). The average cell number in disseminated cell clusters was higher in radially aligned fibers (MCF7: 3.76, T47D: 3.08) than in circumferentially oriented fibers (MCF7: 1.43, T47D: 1.35) (Figure 6E).

Our aligned collagen gel can also be applied to investigate individual cell behaviors. When cancer cells were seeded as individual cells in collagen gels aligned by Couette flow and gravity, individual cells were surrounded by aligned fibers instead of dual topography. After a 7-day culture in aligned fibers, tumor cells formed elongated multicellular clusters along the orientation of aligned fibers, similar to the disseminated cell clusters in dual topographical spheroid models (Supplementary Figure 3). In summary, our dual topographical tumor spheroid model with disseminated tumor clusters invades along radially aligned fibers and recapitulates the histology of tumor invasion in human cancer.

3.6. Dual topographical tumor model distinguishes invasion pattern of tumor spheroids and organoids

To evaluate whether our dual topographical model can distinguish tumors with different invasive and metastatic potentials, we investigated breast tumor spheroid or organoid models differing in ER/PR/HER2 status and invasion ability. Tumor spheroids were originated from T47D and MDAMB231 human breast cancer cells. Tumor organoids were derived from mouse mammary tumor models, MMTV-PyMT [41] and C3(1)-Tag [42]. T47D represents a luminal A (ER⁺/PR^{+/-}/HER2⁻) subtype and is minimally invasive [50, 51]. MMTV-PyMT represents a luminal B (ER⁺/PR^{+/-}/HER2⁺) subtype and is moderately invasive. Both MDAMB231 and C3(1)-Tag represent the basal triple-negative (ER⁻/PR⁻/HER2⁻) subtype are highly invasive *in vivo* [52]. After four days of invasion in our dual topographical tumor model, tumor spheroids/organoids from the different models displayed different invasion patterns responding to local fiber structures. In radial zones, all four tumor spheroid/organoid models invaded with finger-like projections and disseminated cell clusters along radially aligned fibers (Figure 7A and 7B; Supplementary Movie 5 and 6). Fiber orientation in radial zones retained radial alignment in all four tumor spheroids/organoids (Figure 7C). Moreover, MMTV-PyMT, MDAMB231, and C3(1)-Tag spheroids/organoids, which are metastatic *in vivo*, had significantly higher border complexities and more disseminated cell clusters compared to T47D spheroids, which is non-metastatic *in vivo* (Figure 7D and 7E). In the circumferential zone, basal-like tumor spheroids/organoids, MDAMB231 and C3(1)-Tag remodeled collagen fibers to be radially aligned (Figure 7C). On the contrary, T47D and MMTV-PyMT spheroids/organoids failed to remodel circumferentially oriented structures. In the circumferential zone, MDAMB231 and C3(1)-Tag spheroids/organoids demonstrated higher border complexity than T47D spheroids (Figure 7D). C3(1)-Tag organoids had more disseminated cell clusters than T47D and MMTV-PyMT spheroids/organoids (Figure 7E).

Allowing tumor spheroids/organoids to interact with both radially aligned and circumferentially oriented topography, our dual topographical tumor model further revealed how different tumors react uniquely to local topography. Compared to the circumferentially oriented side, radially aligned topography significantly increased border complexity and disseminated cell cluster number in MMTV-PyMT, MDAMB231, and C3(1)-Tag spheroids/organoids and T47D spheroids (Figure 7D and 7E). Interestingly, while this enhancement induced by radially aligned topography was observed in all the four tumor spheroids/organoid models, topography-induced collective invasion was more significant in MMTV-PyMT and MDAMB231 spheroids/organoids (Figure 7F). We summarize the *in vivo* invasiveness, molecular subtypes, and *in vitro* invasion pattern of the tumor spheroids/organoids tested in our dual topographical tumor model in Figure 7G.

4. Discussion

Extracellular matrix (ECM), the natural scaffold surrounding tumors, influences cancer cell behavior. A readily fabricated model recapitulating the interaction between tumors and ECM structures is of great interest in understanding how ECM regulates tumor invasion and identifying invasion-specific therapeutic targets. In the present study, we develop a topographical matrix by applying distinct forces specific for each collagen polymerization phase to align collagen fibers. Our 3D dual topographical tumor model enables each tumor spheroid to be surrounded by radially aligned and circumferentially oriented fibers, the two most common topographical features of tumor stroma.

Aligning matrix fibers has gained much interest in the last few decades for its broad application in recapitulating the ECM topography. Properly aligned fibers represent the physiological ECM scaffold features such as heart and skeletal muscle and the pathological features in the tumor microenvironment. However, previous methods of aligning fibers have limitations in their application as 3D tumor spheroid models (Table 1). The cellular contraction method, which aligns collagen fibers by fibroblast-induced strain, requires the decellularization of fibroblasts before seeding target cells [18, 19]. The decellularization step also makes the fabrication process time-consuming and induces potential cytotoxicity in the gel. Electrospinning has been widely used to generate aligned fibers made of natural and artificial materials [53] but requires a bulky machine and cytotoxic crosslinkers [54, 55]. Also, the pore size of densely compacted electrospun fiber scaffolds is too small to embed tumor spheroids [56]. Tumor spheroids can only be seeded onto the fiber sheet surface with a limited number of cells contacting the matrix topography. Techniques used to increase the pore size between electrospun fibers such as salt leaching [57] and sacrificial fiber [58] may change the material properties. Magnetic beads embedded in collagen gels pulled by an external magnetic field to guide fiber assembly direction is another method to align fibers [29]. However, the cytotoxicity and autofluorescence of magnetic beads diminish their application as tumor models [59]. Fluid flow is another commonly applied method to align fibers [31–33]. The shear force generated by laminar flow in the microfluidic devices helps control the anisotropic elongation of fibers [32]. However, the flow in microscale channels may be significantly disturbed by tumor spheroids, limiting the usage of microfluidics as tumor spheroid models. Finally, although the extensional strain method generates a highly aligned collagen sheet, the collagen layer is coated on thin films. Tumor spheroids cannot

Author Manuscript

Author Manuscript

Author Manuscript

be embedded to create a 3D model on such a thin collagen layer [24, 60]. Extensional strain driven by a rotating acupuncture needle in a polymerized collagen gel generates radially aligned fibers centering on the needle [61, 62]. However, highly aligned fibers are only seen in the area close to the needle. The fiber directionality decreases with distance from the needle, making homogeneous alignment difficult [62]. Our 3D dual topography system has several advantages to overcome the limitations of these conventional methods. First, the phase-specific forces we apply to enhance the fiber alignment are achieved within the same device without time delay or sample transfer between devices. Second, our method does not require additional reagents or post-polymerization treatment, thus a cytotoxic-free large-scale collagen gel with anisotropic aligned fibrils can be rapidly generated. Third, a coaxial rotating cylinder system allows pre-seeded tumor spheroids to be surrounded directly by predisposed structures without damaging fiber architecture. Furthermore, our method to fabricate aligned collagen gel can also be applied beyond cancer research. For example, our approach has potential in large-scale tissue engineering which aligned structure is required or in recapitulating tube-shaped organs such as the cardiovascular system.

Author Manuscript

Author Manuscript

Author Manuscript

Studies based on 3D hydrogel models [18, 34] or quasi 3D topographical substrates [63, 64] reported that radially aligned matrix topography enhanced tumor invasion and migration. In these models, however, tumor spheroids were not closely surrounded by the predisposed matrix structures, a unique histological pattern of tumor invasion in human cancer. For example, tumor invasion was not observed in weakly invasive breast tumors such as MCF7 and T47D cells in a hydrogel model, which has pre-aligned collagen fibers only in a restricted area [20]. In a recent study [65], MCF7 spheroids invaded in laser-ablated microtracks in dense collagen, the interface between collagen and culture dish, fibroblast-rich dense collagen, and randomly oriented low-density collagen (1.6 mg/ml). Guidance cues are presented to study cancer invasion in response to ECM microarchitecture in both previous [65] and our present study. The previous study focuses on generating confined space to show that high ECM confinement rescues cell-cell junctions and leads to collective invasion [65]. By comparison, our 3D model is characterized by two different predisposed ECM structures, radially aligned and circumferentially oriented fibers and it demonstrates that tumor matrix topography is a determining factor in cancer invasion of both highly invasive and weakly invasive breast tumors. Moreover, cancer cells are known to react with local mechanical properties such as stiffness [66]. Our model places each tumor spheroid/organoid in direct contact with two different ECM structures at the same local fiber density within the same gel to provide direct proof of topography-induced collective cancer invasion.

Author Manuscript

Author Manuscript

Recent studies revealed that tumors invade as multicellular clusters by retaining E-cadherin expression to carry more metastatic potential [67–69]. In histopathology of human cancer, tumor cluster dissemination or tumor budding is defined by cell clusters of usually less than four or five tumor cells breaking apart from the main tumor [70]. Tumor budding is correlated with poor prognosis, larger tumor size, frequent lymph node metastasis, and distant metastasis in breast cancer [71], colorectal cancer [70], pancreatic cancer [72], gastric cancer [73], and other cancer types [74, 75]. More importantly, a recent prospective randomized controlled study reported that cancer patients with tumor budding have significantly higher tumor recurrence rates when treated with surgery alone compared to

additional postoperative chemotherapy [76]. These findings indicate the clinical implication of disseminated tumor clusters in deciding treatment strategies for cancer patients.

Tumor cluster dissemination in aligned breast tumor stroma is a metastasis precursor, however, mechanisms for the formation of disseminated tumor clusters are unclear. Partial epithelial-mesenchymal transition (EMT) is a generally accepted mechanism of tumor budding [77]. Instead of undergoing a complete EMT, cancer cells have the plasticity of retaining both epithelial and mesenchymal characteristics to invade as small cell clusters [77]. Our current study demonstrates that radially aligned topography acts as an external biophysical cue that promotes tumor cluster dissemination in luminal A (T47D), luminal B (MMTV-PyMT), and basal (MDAMB231 and C3(1)-Tag) subtypes of breast cancer. In mesenchymal-type tumor cells, a high-density ECM caused cell jamming and facilitated cluster formation [78]. However, in our dual topographical model, both radially aligned and circumferentially oriented fibers are within the same gel and have the same fiber density. Therefore, ECM topography can be an independent factor in driving collective cell invasion and cell cluster dissemination in both epithelial and mesenchymal-type cancer and may have distinct mechanisms other than EMT or cell jamming. Several possible mechanisms include Rho/ROCK signaling of cell contractility, cell-cell adhesion regulation aside from EMT, or integrin mechanotransduction involved in cell-matrix interaction. Rho/ROCK signaling-mediated cell contractility was shown to play an essential role for tumors to align surrounding matrix fibers [17, 79]. But after the fibers are remodeled, the invasion of MDAMB231 cells in aligned fibers no longer needs Rho/ROCK mediated contractility [17]. It is not clear whether the invasion of weakly invasive tumors such as T47D and MCF7 in pre-aligned fibers is independent of Rho/ROCK signaling. An alternative mechanism of collective cluster dissemination is an activation of the developmental pathway. A re-acquired expression of adhesion molecules by plakoglobin [68], keratin 14 [69], or CD44 upregulation [80] holds tumor cells together and increases the survival of tumor clusters in circulation. Cancer cell invasion in ECM fibers is also extensively affected by the integrin-regulated interaction between cells and collagen fibers [81]. It is still unknown whether and how cell-cell adhesion or cell-matrix adhesion mediates topography-induced collective invasion. These unresolved questions reinforce our new 3D model as a *in vivo*-like platform for elucidating the mechanism of topography-induced tumor cluster dissemination.

5. Conclusion

We developed a rapid and reproducible method to fabricate a 3D dual topographical tumor model in which tumor spheroids are surrounded by two common predisposed tumor ECM structures, radially aligned and circumferentially oriented collagen fibers. Radially aligned topography promotes multicellular cluster-dissemination detached from the main tumor, which recapitulates *in vivo* cancer invasion. Our 3D tumor model is a viable experimental platform for investigating tumor invasion and identifying therapeutic targets against metastasis.

Supplementary Material

Refer to Web version on PubMed Central for supplementary material.

Acknowledgments

This work was supported by grants from the Human Frontier Science Program (RGP0038/2018) (to D.-H.Kim), the Ministry of Trade, Industry and Energy (MOTIE) and Korea Institute for Advancement of Technology (KIAT) through the International Cooperative R&D program (Project No. P0004638) and NCI R21 CA220111 of the National Institutes of Health (NIH) (to EH Ahn). A.J.E. received support for this project through grants from: the Breast Cancer Research Foundation (BCRF-20-048), the Jayne Koskinas Ted Giovanis Foundation for Health and Policy, and the National Institutes of Health / National Cancer Institute (U01CA217846, U54CA2101732, 3P30CA006973). The authors thank Dr. Chibum Lee, Seoul National University of Science and Technology, for suggesting device design. The authors thank Dr. Christopher Miller, Fred Hutchinson Cancer Research Center, for critically reading and editing the manuscript.

Data availability

The data are available from the corresponding author on reasonable request.

References

- [1]. Kai F, Drain AP, Weaver VM, The Extracellular Matrix Modulates the Metastatic Journey, *Dev Cell*49(3) (2019) 332–346. [PubMed: 31063753]
- [2]. Giussani M, Merlino G, Cappelletti V, Tagliabue E, Daidone MG, Tumor-extracellular matrix interactions: Identification of tools associated with breast cancer progression, *Semin Cancer Biol*35 (2015) 3–10. [PubMed: 26416466]
- [3]. Kaushik S, Pickup MW, Weaver VM, From transformation to metastasis: deconstructing the extracellular matrix in breast cancer, *Cancer Metastasis Rev*35(4) (2016) 655–667. [PubMed: 27914000]
- [4]. Chin AR, Wang SE, Cancer Tills the Premetastatic Field: Mechanistic Basis and Clinical Implications, *Clin Cancer Res*22(15) (2016) 3725–33. [PubMed: 27252414]
- [5]. Liu Y, Cao X, Characteristics and Significance of the Pre-metastatic Niche, *Cancer Cell*30(5) (2016) 668–681. [PubMed: 27846389]
- [6]. Friedl P, Alexander S, Cancer invasion and the microenvironment: plasticity and reciprocity, *Cell*147(5) (2011) 992–1009. [PubMed: 22118458]
- [7]. Cox TR, Erler JT, Remodeling and homeostasis of the extracellular matrix: implications for fibrotic diseases and cancer, *Dis Model Mech*4(2) (2011) 165–78. [PubMed: 21324931]
- [8]. Malik R, Lelkes PI, Cukierman E, Biomechanical and biochemical remodeling of stromal extracellular matrix in cancer, *Trends Biotechnol*33(4) (2015) 230–6. [PubMed: 25708906]
- [9]. Riching KM, Cox BL, Salick MR, Pehlke C, Riching AS, Ponik SM, Bass BR, Crone WC, Jiang Y, Weaver AM, Eliceiri KW, Keely PJ, 3D collagen alignment limits protrusions to enhance breast cancer cell persistence, *Biophys J*107(11) (2014) 2546–58. [PubMed: 25468334]
- [10]. Alexander S, Weigelin B, Winkler F, Friedl P, Preclinical intravital microscopy of the tumour-stroma interface: invasion, metastasis, and therapy response, *Curr Opin Cell Biol*25(5) (2013) 659–71. [PubMed: 23896198]
- [11]. Mayorca-Guiliani AE, Madsen CD, Cox TR, Horton ER, Venning FA, Erler JT, ISDoT: in situ decellularization of tissues for high-resolution imaging and proteomic analysis of native extracellular matrix, *Nat Med*23(7) (2017) 890–898. [PubMed: 28604702]
- [12]. Ma XJ, Dahiya S, Richardson E, Erlander M, Sgroi DC, Gene expression profiling of the tumor microenvironment during breast cancer progression, *Breast Cancer Res*11(1) (2009) R7. [PubMed: 19187537]
- [13]. Conklin MW, Gangnon RE, Sprague BL, Van Gemert L, Hampton JM, Eliceiri KW, Bredfeldt JS, Liu Y, Surachaicharn N, Newcomb PA, Friedl A, Keely PJ, Trentham-Dietz A, Collagen Alignment as a Predictor of Recurrence after Ductal Carcinoma In Situ, *Cancer Epidemiol Biomarkers Prev*27(2) (2018) 138–145. [PubMed: 29141852]
- [14]. Lyons TR, O'Brien J, Borges VF, Conklin MW, Keely PJ, Eliceiri KW, Marusyk A, Tan AC, Schedin P, Postpartum mammary gland involution drives progression of ductal carcinoma in situ through collagen and COX-2, *Nat Med*17(9) (2011) 1109–15. [PubMed: 21822285]

- [15]. Levental KR, Yu H, Kass L, Lakins JN, Egeblad M, Erler JT, Fong SF, Csiszar K, Giaccia A, Weninger W, Yamauchi M, Gasser DL, Weaver VM, Matrix crosslinking forces tumor progression by enhancing integrin signaling, *Cell*139(5) (2009) 891–906. [PubMed: 19931152]
- [16]. Balcioglu HE, van de Water B, Danen EH, Tumor-induced remote ECM network orientation steers angiogenesis, *Sci Rep*6 (2016) 22580. [PubMed: 26931404]
- [17]. Provenzano PP, Inman DR, Eliceiri KW, Trier SM, Keely PJ, Contact guidance mediated three-dimensional cell migration is regulated by Rho/ROCK-dependent matrix reorganization, *Biophys J*95(11) (2008) 5374–84. [PubMed: 18775961]
- [18]. Ray A, Morford RK, Ghaderi N, Odde DJ, Provenzano PP, Dynamics of 3D carcinoma cell invasion into aligned collagen, *Integr Biol (Camb)*10(2) (2018) 100–112. [PubMed: 29340409]
- [19]. Ray A, Slama ZM, Morford RK, Madden SA, Provenzano PP, Enhanced Directional Migration of Cancer Stem Cells in 3D Aligned Collagen Matrices, *Biophys J*112(5) (2017) 1023–1036. [PubMed: 28297639]
- [20]. Han W, Chen S, Yuan W, Fan Q, Tian J, Wang X, Chen L, Zhang X, Wei W, Liu R, Qu J, Jiao Y, Austin RH, Liu L, Oriented collagen fibers direct tumor cell intravasation, *Proc Natl Acad Sci U S A*113(40) (2016) 11208–11213. [PubMed: 27663743]
- [21]. Gong X, Kulwatno J, Mills KL, Rapid fabrication of collagen bundles mimicking tumor-associated collagen architectures, *Acta Biomater* (2020).
- [22]. Yang Y, Zheng H, Zhan Y, Fan S, An emerging tumor invasion mechanism about the collective cell migration, *Am J Transl Res*11(9) (2019) 5301–5312. [PubMed: 31632511]
- [23]. Vader D, Kabla A, Weitz D, Mahadevan L, Strain-induced alignment in collagen gels, *PLoS One*4(6) (2009) e5902. [PubMed: 19529768]
- [24]. Nam E, Lee WC, Takeuchi S, Formation of Highly Aligned Collagen Nanofibers by Continuous Cyclic Stretch of a Collagen Hydrogel Sheet, *Macromol Biosci*16(7) (2016) 995–1000. [PubMed: 27136124]
- [25]. Ricking KM, Cox BL, Salick MR, Pehlke C, Ricking AS, Ponik SM, Bass BR, Crone WC, Jiang Y, Weaver AM, Eliceiri KW, Keely PJ, 3D Collagen Alignment Limits Protrusions to Enhance Breast Cancer Cell Persistence, *Biophysical Journal*107(11) (2014) 2546–2558. [PubMed: 25468334]
- [26]. Matthews JA, Wnek GE, Simpson DG, Bowlin GL, Electrospinning of collagen nanofibers, *Biomacromolecules*3(2) (2002) 232–8. [PubMed: 11888306]
- [27]. Rho KS, Jeong L, Lee G, Seo BM, Park YJ, Hong SD, Roh S, Cho JJ, Park WH, Min BM, Electrospinning of collagen nanofibers: effects on the behavior of normal human keratinocytes and early-stage wound healing, *Biomaterials*27(8) (2006) 1452–61. [PubMed: 16143390]
- [28]. Zhong S, Teo WE, Zhu X, Beuerman RW, Ramakrishna S, Yung LY, An aligned nanofibrous collagen scaffold by electrospinning and its effects on in vitro fibroblast culture, *J Biomed Mater Res A*79(3) (2006) 456–63. [PubMed: 16752400]
- [29]. Dickinson RB, Guido S, Tranquillo RT, Biased cell migration of fibroblasts exhibiting contact guidance in oriented collagen gels, *Ann Biomed Eng*22(4) (1994) 342–56. [PubMed: 7998680]
- [30]. Guo C, Kaufman LJ, Flow and magnetic field induced collagen alignment, *Biomaterials*28(6) (2007) 1105–14. [PubMed: 17112582]
- [31]. Lanfer B, Freudenberg U, Zimmermann R, Stamo D, Korber V, Werner C, Aligned fibrillar collagen matrices obtained by shear flow deposition, *Biomaterials*29(28) (2008) 3888–3895. [PubMed: 18606448]
- [32]. Saeidi N, Sander EA, Ruberti JW, Dynamic shear-influenced collagen self-assembly, *Biomaterials*30(34) (2009) 6581–92. [PubMed: 19765820]
- [33]. Burkel B, Morris BA, Ponik SM, Ricking KM, Eliceiri KW, Keely PJ, Preparation of 3D Collagen Gels and Microchannels for the Study of 3D Interactions In Vivo, *J Vis Exp* (111) (2016).
- [34]. Gjorevski N, Piotrowski AS, Varner VD, Nelson CM, Dynamic tensile forces drive collective cell migration through three-dimensional extracellular matrices, *Sci Rep*5 (2015) 11458. [PubMed: 26165921]
- [35]. Agudelo-Garcia PA, De Jesus JK, Williams SP, Nowicki MO, Chiocca EA, Liyanarachchi S, Li PK, Lannutti JJ, Johnson JK, Lawler SE, Viapiano MS, Glioma cell migration on three-

dimensional nanofiber scaffolds is regulated by substrate topography and abolished by inhibition of STAT3 signaling, *Neoplasia*13(9) (2011) 831–40. [PubMed: 21969816]

- [36]. Gale M, Pollanen MS, Markiewicz P, Goh MC, Sequential assembly of collagen revealed by atomic force microscopy, *Biophys J*68(5) (1995) 2124–8. [PubMed: 7612856]
- [37]. Holloway CR, Dyson RJ, Smith DJ, Linear Taylor-Couette stability of a transversely isotropic fluid, *Proceedings of the Royal Society A: Mathematical, Physical and Engineering Sciences*471(2178) (2015) 20150141.
- [38]. Bredfeldt JS, Liu Y, Pehlke CA, Conklin MW, Szulczewski JM, Inman DR, Keely PJ, Nowak RD, Mackie TR, Eliceiri KW, Computational segmentation of collagen fibers from second-harmonic generation images of breast cancer, *J Biomed Opt*19(1) (2014) 16007. [PubMed: 24407500]
- [39]. Berens P, *CircStat: A MATLAB Toolbox for Circular Statistics*, 2009 31(10) (2009) 21.
- [40]. Razian G, Yu Y, Ungrin M, Production of large numbers of size-controlled tumor spheroids using microwell plates, *J Vis Exp* (81) (2013) e50665. [PubMed: 24300192]
- [41]. Guy CT, Cardiff RD, Muller WJ, Induction of mammary tumors by expression of polyomavirus middle T oncogene: a transgenic mouse model for metastatic disease, *Mol Cell Biol*12(3) (1992) 954–61. [PubMed: 1312220]
- [42]. Maroulakou IG, Anver M, Garrett L, Green JE, Prostate and mammary adenocarcinoma in transgenic mice carrying a rat C3(1) simian virus 40 large tumor antigen fusion gene, *Proc Natl Acad Sci U S A*91(23) (1994) 11236–40. [PubMed: 7972041]
- [43]. Padmanaban V, Grasset EM, Neumann NM, Fraser AK, Henriot E, Matsui W, Tran PT, Cheung KJ, Georgess D, Ewald AJ, Organotypic culture assays for murine and human primary and metastatic-site tumors, *Nat Protoc*15(8) (2020) 2413–2442. [PubMed: 32690957]
- [44]. Hou Y, Konen J, Brat DJ, Marcus AI, Cooper LAD, TASI: A software tool for spatial-temporal quantification of tumor spheroid dynamics, *Sci Rep*8(1) (2018) 7248. [PubMed: 29739990]
- [45]. Oskarsson T, Extracellular matrix components in breast cancer progression and metastasis, *Breast*22Suppl 2 (2013) S66–72. [PubMed: 24074795]
- [46]. Jena MK, Janjanam J, Role of extracellular matrix in breast cancer development: a brief update, *F1000Res*7 (2018) 274. [PubMed: 29983921]
- [47]. Fuchs HL, Christman AJ, Gerbi GP, Hunter EJ, Diez FJ, Directional flow sensing by passively stable larvae, *J Exp Biol*218(Pt 17) (2015) 2782–92. [PubMed: 26333930]
- [48]. Hirshfeld D, Rapaport DC, Growth of Taylor vortices: A molecular dynamics study, *Phys Rev E Stat Phys Plasmas Fluids Relat Interdiscip Topics*61(1) (2000) R21–4. [PubMed: 11046363]
- [49]. Hadjipanayi E, Mudera V, Brown RA, Guiding cell migration in 3D: a collagen matrix with graded directional stiffness, *Cell Motil Cytoskeleton*66(3) (2009) 121–8. [PubMed: 19170223]
- [50]. Rizwan A, Cheng M, Bhujwala ZM, Krishnamachary B, Jiang L, Glunde K, Breast cancer cell adhesion and degradation interact to drive metastasis, *NPJ Breast Cancer*1 (2015) 15017. [PubMed: 28721370]
- [51]. Holliday DL, Speirs V, Choosing the right cell line for breast cancer research, *Breast Cancer Res*13(4) (2011) 215. [PubMed: 21884641]
- [52]. Herschkowitz JI, Simin K, Weigman VJ, Mikaelian I, Usary J, Hu Z, Rasmussen KE, Jones LP, Assefnia S, Chandrasekharan S, Backlund MG, Yin Y, Khramtsov AI, Bastein R, Quackenbush J, Glazer RI, Brown PH, Green JE, Kopelovich L, Furth PA, Palazzo JP, Olopade OI, Bernard PS, Churchill GA, Van Dyke T, Perou CM, Identification of conserved gene expression features between murine mammary carcinoma models and human breast tumors, *Genome Biol*8(5) (2007) R76. [PubMed: 17493263]
- [53]. Xue J, Xie J, Liu W, Xia Y, *Electrospun Nanofibers: New Concepts, Materials, and Applications*, *Acc Chem Res*50(8) (2017) 1976–1987. [PubMed: 28777535]
- [54]. Tirella A, Liberto T, Ahluwalia A, Riboflavin and collagen: New crosslinking methods to tailor the stiffness of hydrogels, *Mater Lett*74 (2012) 58–61.
- [55]. Itoh S, Takakuda K, Kawabata S, Aso Y, Kasai K, Itoh H, Shinomiya K, Evaluation of cross-linking procedures of collagen tubes used in peripheral nerve repair, *Biomaterials*23(23) (2002) 4475–4481. [PubMed: 12322967]

- [56]. Wu J, Hong Y, Enhancing cell infiltration of electrospun fibrous scaffolds in tissue regeneration, *Bioact Mater*1(1) (2016) 56–64. [PubMed: 29744395]
- [57]. Kim TG, Chung HJ, Park TG, Macroporous and nanofibrous hyaluronic acid/collagen hybrid scaffold fabricated by concurrent electrospinning and deposition/leaching of salt particles, *Acta Biomater*4(6) (2008) 1611–9. [PubMed: 18640884]
- [58]. Phipps MC, Clem WC, Grunda JM, Clines GA, Bellis SL, Increasing the pore sizes of bone-mimetic electrospun scaffolds comprised of polycaprolactone, collagen I and hydroxyapatite to enhance cell infiltration, *Biomaterials*33(2) (2012) 524–34. [PubMed: 22014462]
- [59]. Yaman S, Anil-Inevi M, Ozcivici E, Tekin HC, Magnetic Force-Based Microfluidic Techniques for Cellular and Tissue Bioengineering, *Front Bioeng Biotechnol*6 (2018) 192. [PubMed: 30619842]
- [60]. Chaubaroux C, Perrin-Schmitt F, Senger B, Vidal L, Voegel JC, Schaaf P, Haikel Y, Boulmedais F, Lavalle P, Hemmerle J, Cell Alignment Driven by Mechanically Induced Collagen Fiber Alignment in Collagen/Alginate Coatings, *Tissue Eng Part C Methods*21(9) (2015) 881–8. [PubMed: 25658028]
- [61]. Julias M, Edgar LT, Buettner HM, Shreiber DI, An in vitro assay of collagen fiber alignment by acupuncture needle rotation, *Biomed Eng Online*7 (2008) 19. [PubMed: 18606012]
- [62]. Nuhn JAM, Perez AM, Schneider IC, Contact guidance diversity in rotationally aligned collagen matrices, *Acta Biomater*66 (2018) 248–257. [PubMed: 29196116]
- [63]. Ray A, Lee O, Win Z, Edwards RM, Alford PW, Kim DH, Provenzano PP, Anisotropic forces from spatially constrained focal adhesions mediate contact guidance directed cell migration, *Nat Commun*8 (2017) 14923. [PubMed: 28401884]
- [64]. Nam KH, Kim P, Wood DK, Kwon S, Provenzano PP, Kim DH, Multiscale Cues Drive Collective Cell Migration, *Sci Rep*6 (2016) 29749. [PubMed: 27460294]
- [65]. Ilina O, Gritsenko PG, Syga S, Lippoldt J, La Porta CAM, Chepizhko O, Grosser S, Vullings M, Bakker GJ, Starruss J, Bult P, Zapperi S, Kas JA, Deutsch A, Friedl P, Cell-cell adhesion and 3D matrix confinement determine jamming transitions in breast cancer invasion, *Nat Cell Biol*22(9) (2020) 1103–1115. [PubMed: 32839548]
- [66]. Nia HT, Munn LL, Jain RK, Physical traits of cancer, *Science*370(6516) (2020).
- [67]. Padmanaban V, Krol I, Suhail Y, Szczerba BM, Aceto N, Bader JS, Ewald AJ, E-cadherin is required for metastasis in multiple models of breast cancer, *Nature*573(7774) (2019) 439–444. [PubMed: 31485072]
- [68]. Aceto N, Bardia A, Miyamoto DT, Donaldson MC, Wittner BS, Spencer JA, Yu M, Pely A, Engstrom A, Zhu H, Brannigan BW, Kapur R, Stott SL, Shioda T, Ramaswamy S, Ting DT, Lin CP, Toner M, Haber DA, Maheswaran S, Circulating tumor cell clusters are oligoclonal precursors of breast cancer metastasis, *Cell*158(5) (2014) 1110–1122. [PubMed: 25171411]
- [69]. Cheung KJ, Padmanaban V, Silvestri V, Schipper K, Cohen JD, Fairchild AN, Gorin MA, Verdone JE, Pienta KJ, Bader JS, Ewald AJ, Polyclonal breast cancer metastases arise from collective dissemination of keratin 14-expressing tumor cell clusters, *Proc Natl Acad Sci U S A*113(7) (2016) E854–63. [PubMed: 26831077]
- [70]. Lugli A, Kirsch R, Ajioka Y, Bosman F, Cathomas G, Dawson H, El Zimaity H, Flejou JF, Hansen TP, Hartmann A, Kakar S, Langner C, Nagtegaal I, Puppa G, Riddell R, Ristimaki A, Sheahan K, Smyrk T, Sugihara K, Terris B, Ueno H, Vieth M, Zlobec I, Quirke P, Recommendations for reporting tumor budding in colorectal cancer based on the International Tumor Budding Consensus Conference (ITBCC) 2016, *Mod Pathol*30(9) (2017) 1299–1311. [PubMed: 28548122]
- [71]. Gujam FJ, McMillan DC, Mohammed ZM, Edwards J, Going JJ, The relationship between tumour budding, the tumour microenvironment and survival in patients with invasive ductal breast cancer, *Br J Cancer*113(7) (2015) 1066–74. [PubMed: 26263482]
- [72]. O'Connor K, Li-Chang HH, Kalloger SE, Peixoto RD, Webber DL, Owen DA, Driman DK, Kirsch R, Serra S, Scudamore CH, Renouf DJ, Schaeffer DF, Tumor budding is an independent adverse prognostic factor in pancreatic ductal adenocarcinoma, *Am J Surg Pathol*39(4) (2015) 472–8. [PubMed: 25634751]

- [73]. Koelzer VH, Langer R, Zlobec I, Lugli A, Tumor budding in upper gastrointestinal carcinomas, *Front Oncol*4 (2014) 216. [PubMed: 25177546]
- [74]. Rokutan-Kurata M, Yoshizawa A, Nakajima N, Teramoto Y, Sumiyoshi S, Kondo K, Hamaji M, Sonobe M, Menju T, Date H, Haga H, Discohesive growth pattern (Disco-p) as an unfavorable prognostic factor in lung adenocarcinoma: an analysis of 1062 Japanese patients with resected lung adenocarcinoma, *Mod Pathol* (2020).
- [75]. Almangush A, Salo T, Hagstrom J, Leivo I, Tumour budding in head and neck squamous cell carcinoma - a systematic review, *Histopathology*65(5) (2014) 587–94. [PubMed: 24897954]
- [76]. Ueno H, Ishiguro M, Nakatani E, Ishikawa T, Uetake H, Matsuda C, Nakamoto Y, Kotake M, Kurachi K, Egawa T, Yasumasa K, Murata K, Ikawa O, Shinji S, Murotani K, Matsui S, Teramukai S, Tomita N, Sugihara K, Group SS, Prospective Multicenter Study on the Prognostic and Predictive Impact of Tumor Budding in Stage II Colon Cancer: Results From the SACURA Trial, *J Clin Oncol*37(22) (2019) 1886–1894. [PubMed: 31180819]
- [77]. Grigore AD, Jolly MK, Jia D, Farach-Carson MC, Levine H, Tumor Budding: The Name is EMT. Partial EMT, *J Clin Med*5(5) (2016).
- [78]. Haeger A, Krause M, Wolf K, Friedl P, Cell jamming: collective invasion of mesenchymal tumor cells imposed by tissue confinement, *Biochim Biophys Acta*1840(8) (2014) 2386–95. [PubMed: 24721714]
- [79]. Piotrowski-Daspit AS, Nерger BA, Wolf AE, Sundaresan S, Nelson CM, Dynamics of Tissue-Induced Alignment of Fibrous Extracellular Matrix, *Biophys J*113(3) (2017) 702–713. [PubMed: 28793224]
- [80]. Liu X, Taftaf R, Kawaguchi M, Chang YF, Chen W, Entenberg D, Zhang Y, Gerratana L, Huang S, Patel DB, Tsui E, Adorno-Cruz V, Chirieleison SM, Cao Y, Harney AS, Patel S, Patsialou A, Shen Y, Avril S, Gilmore HL, Lathia JD, Abbott DW, Cristofanilli M, Condeelis JS, Liu H, Homophilic CD44 Interactions Mediate Tumor Cell Aggregation and Polyclonal Metastasis in Patient-Derived Breast Cancer Models, *Cancer Discov*9(1)(2019) 96–113. [PubMed: 30361447]
- [81]. Zeltz C, Gullberg D, The integrin-collagen connection--a glue for tissue repair?, *J Cell Sci*129(4) (2016) 653–64. [PubMed: 26857815]
- [82]. Chen S, Boda SK, Batra SK, Li X, Xie J, Emerging Roles of Electrospun Nanofibers in Cancer Research, *Adv Healthc Mater*7(6) (2018) e1701024. [PubMed: 29210522]
- [83]. Nelson MT, Short A, Cole SL, Gross AC, Winter J, Eubank TD, Lannutti JJ, Preferential, enhanced breast cancer cell migration on biomimetic electrospun nanofiber ‘cell highways’, *BMC Cancer*14 (2014) 825. [PubMed: 25385001]

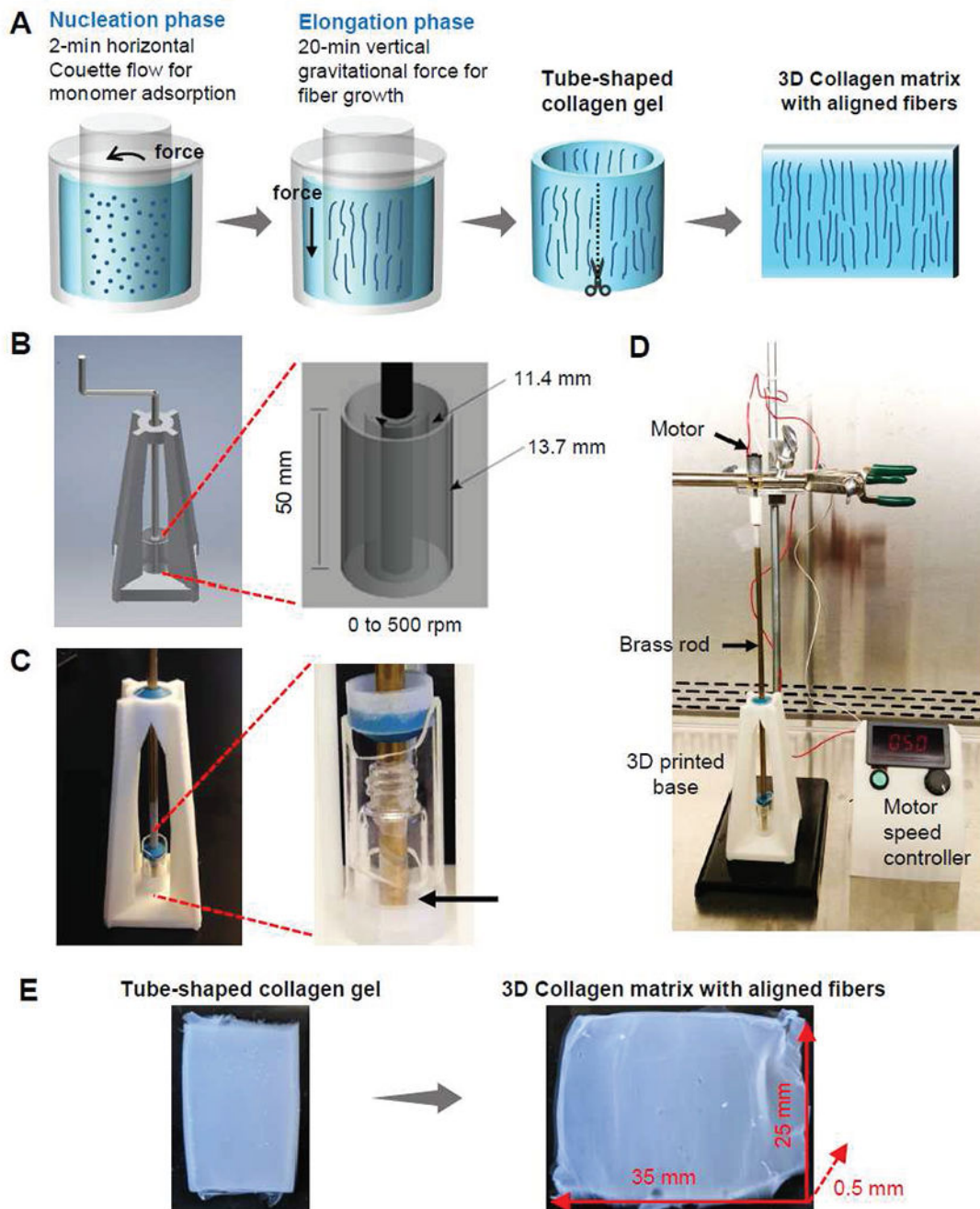


Figure 1. Alignment of collagen fibers by a phase-specific, force-guided method in a coaxial rotating cylinder system.

(A) Proof of concept of a phase-specific, force-guided method. In the nucleation phase, a 2-minute horizontal laminar Couette flow is applied to adsorb collagen monomers on the cylinder glass surfaces. Then, in the elongation phase, the growth of collagen fibers is guided by a vertical gravitational force during a 20-minute gelling in a stationary condition. After an intact tube-shaped collagen gel is generated, the gel is cut and spread to form a large 3D collagen matrix with aligned fibers. A computer-aided design (B) and device

images **(C)** of coaxial rotating cylinder-system. The system consists of two glass cylinders concentrically aligned by a 3D printed base, a brass rod, and plastic bearings. Collagen is polymerized in the space between the two coaxial cylinders (arrow). **(D)** Coaxial rotating cylinder system is powered by a motor and speed controller system. **(E)** A tube-shaped collagen gel is taken out from the coaxial rotating cylinder system. After the tube-shaped collagen gel is cut and spread, a large collagen matrix with aligned fibers is generated.

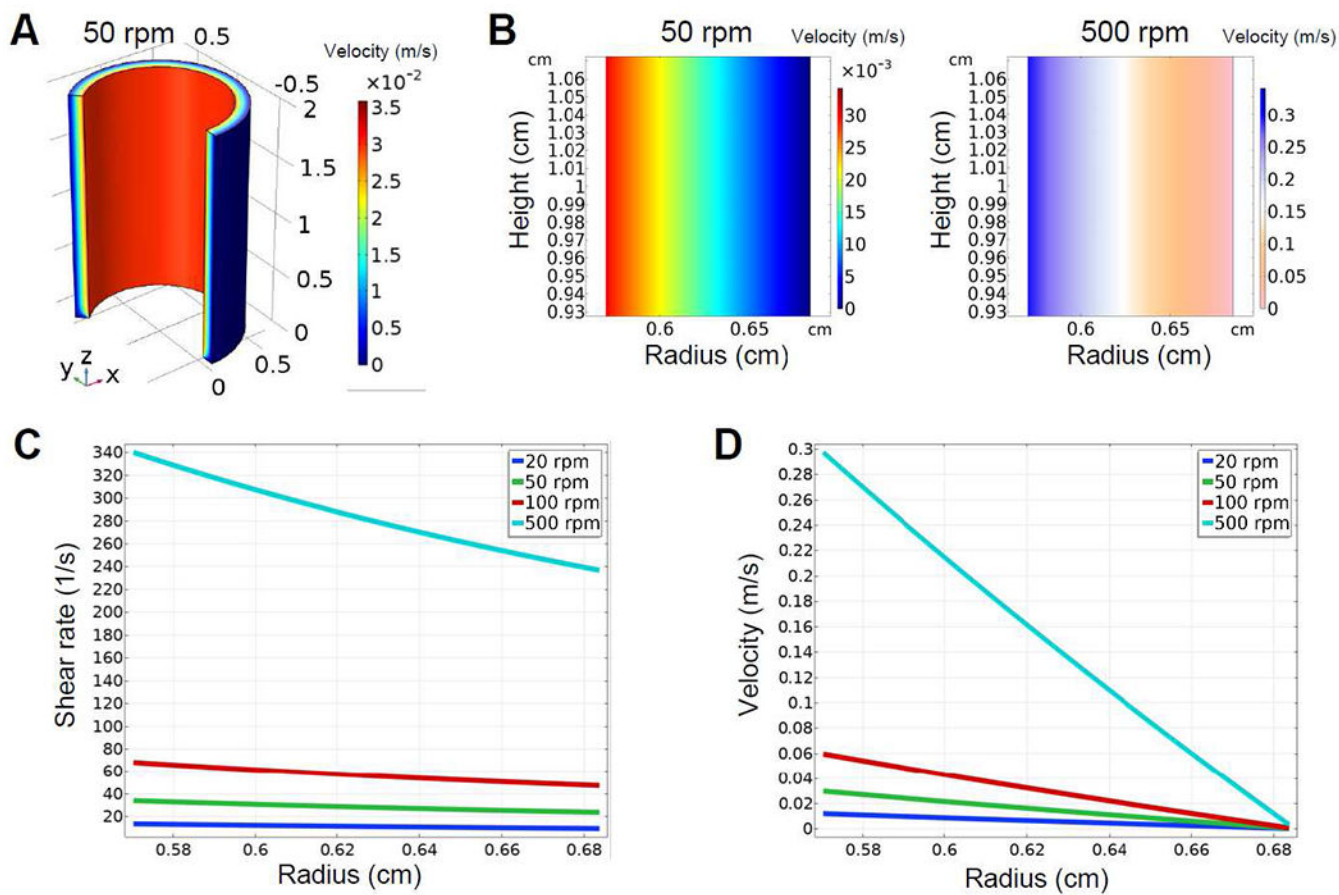


Figure 2. Computational fluid dynamic simulation of laminar Couette flow in collagen solution.

(A) A 3D plot of the fluid velocity field exhibits a laminar Couette flow in collagen solution with the inner cylinder rotating at 50 rpm. (B) 2D plots of the fluid velocity field demonstrates a laminar Couette flow with the inner cylinder rotating at 50 rpm and 500 rpm, respectively. (C and D) The desired shear rate (C) of 35 s^{-1} and flow velocity (D) of 0.03 m/s are identified for the inner cylinder rotation at 50 rpm to align collagen fibers.

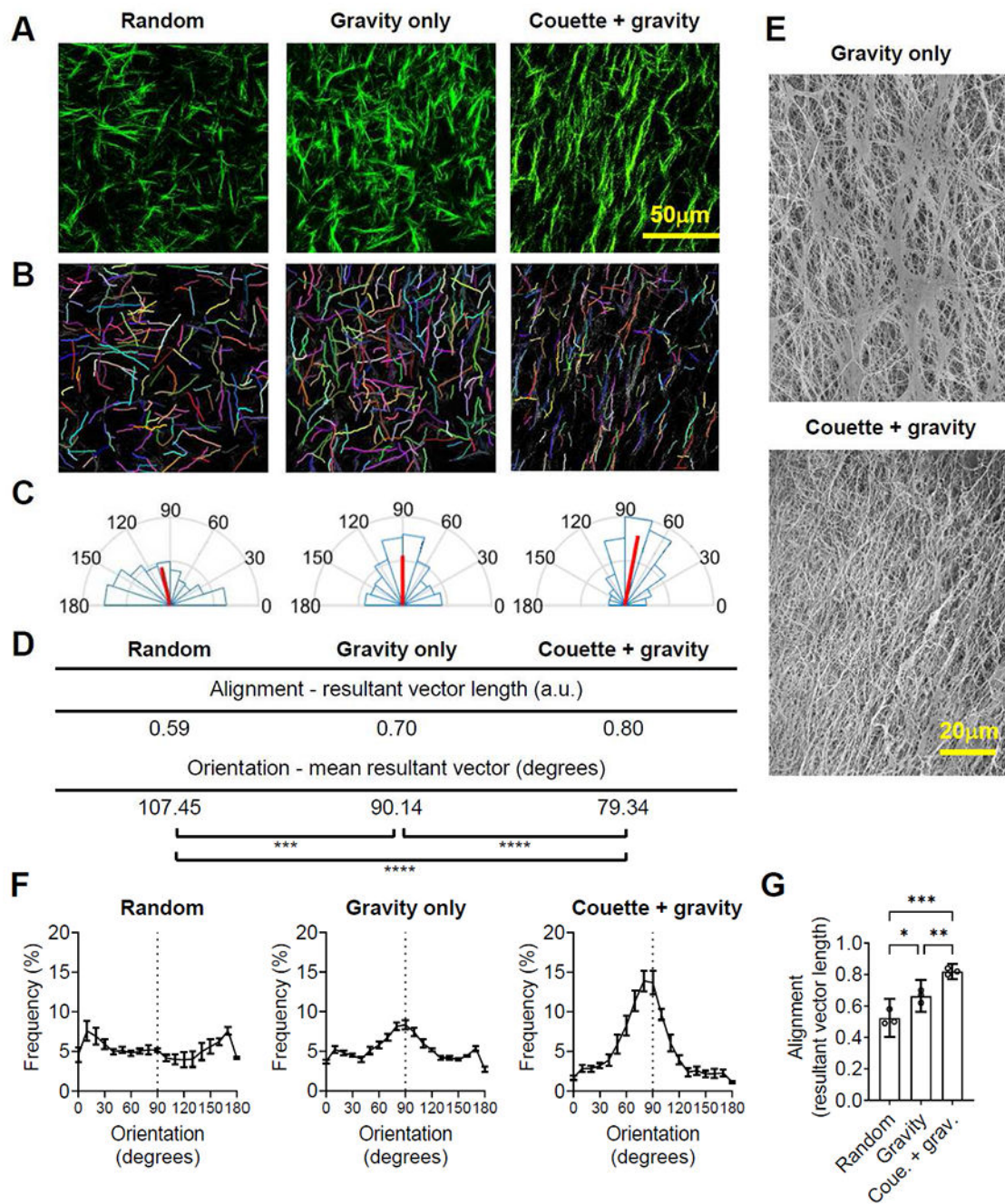


Figure 3. The laminar Couette flow followed by gravitational force enhances fiber alignment.

Images of multiphoton second-harmonic generation (**A**) and computational segments (**B**) of collagen fibers in random (fiber polymerization on a glass slide), gravity only (fiber polymerization by gravitational force only), and Couette + gravity groups (fiber polymerization by laminar Couette flow with subsequent gravitational force). (**C**) The angular frequency distribution of collagen fibers within one gel for each experimental group ($n=20$ images). Red lines represent the magnitude and direction of mean resultant vectors. (**D**) A directional statistics analysis reveals a more aligned but slightly deviated collagen

fiber orientation in a Couette + gravity sample compared to a gravity only sample within one gel for each experimental group (n=20 images). *** $p < 0.001$, **** $p < 0.0001$ by Watson-Williams test. (E) Scanning electron microscope images of collagen fibers exhibit more aligned but oblique-oriented collagen fibers in a Couette + gravity group compared to a gravity only group. (F) Frequency distribution of collagen fiber orientation in random, gravity only, and Couette + gravity groups. Data are mean \pm SEM (20 images per gel from three gels for each experimental group). (G) The resultant vector length of collagen fibers, representing fiber alignment, is greatest in Couette + gravity, followed by gravity only and random groups. Data are mean and 95% confidence interval (CI) (20 images per gel from three gels for each experimental group). * $p < 0.05$, ** $p < 0.01$, *** $p < 0.001$ by one-way ANOVA.

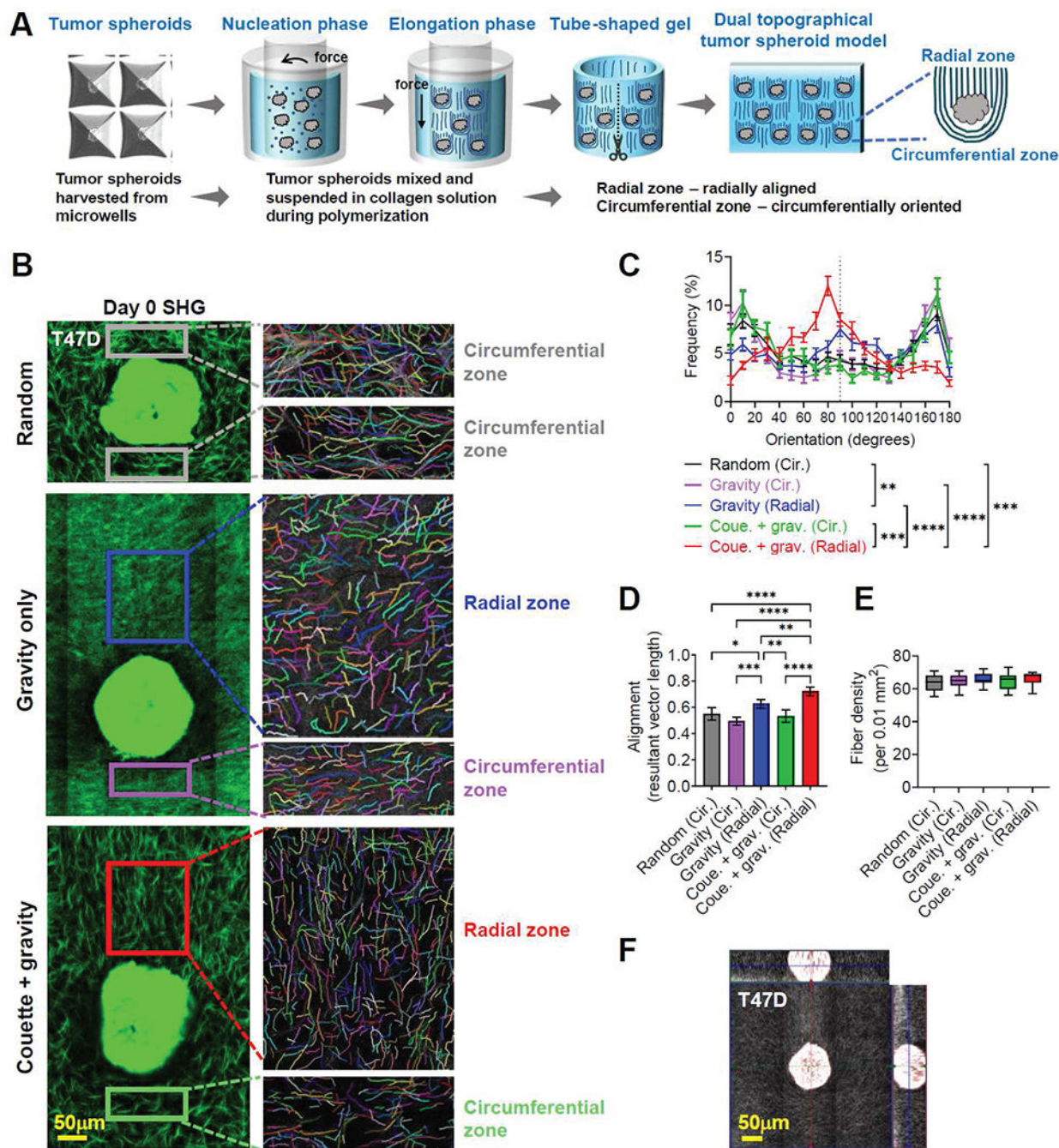


Figure 4. Couette flow with subsequent gravitational force builds a dual topographical tumor spheroid model.

(A) Proof of concept schematic for dual topographical tumor spheroid model. (B) Multiphoton second-harmonic generation and computational segmented images of collagen fibers on day 0 after collagen polymerization with embedded tumor spheroids. (C) Frequency distribution and (D) alignment (resultant vector length) of collagen fiber orientation showing collagen fibers were more aligned in radial zone of tumor spheroids in Couette + gravity group (fiber polymerization by laminar Couette flow with subsequent

gravitational force). **(E)** Fiber density analysis showed no difference in fiber density between circumferential and radial zone in all experimental conditions. **(F)** Orthogonal view of a T47D spheroid on day 0 in Couette + gravity group. **(C)** Data are mean \pm SEM (n=15 spheroids per group from three independent experiments). ** p < 0.01, *** p < 0.001, **** p < 0.0001 by Kolmogorov-Smirnov test for comparing frequency distributions. **(D-E)** Data are mean and 95% CI (n=15 spheroids per group from three independent experiments). * p < 0.05, ** p < 0.01, *** p < 0.001, **** p < 0.0001 by one-way ANOVA.

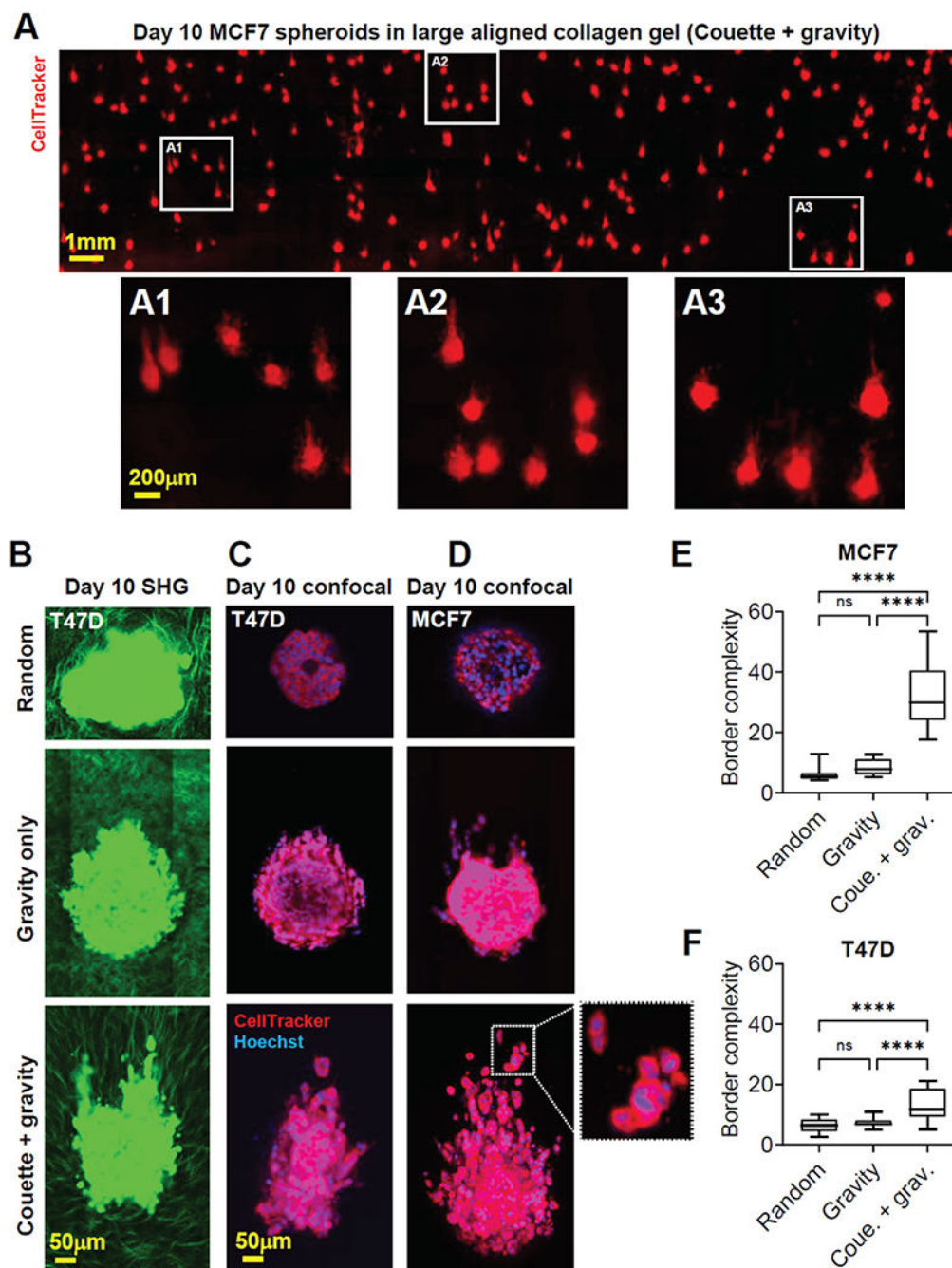


Figure 5. Dual topographical tumor spheroid model reveals cancer invasion pattern determined by matrix topography.

(A) MCF7 spheroids in dual topographical model (fiber polymerization by laminar Couette flow with the subsequent gravitational force) after a 10-day invasion manifests evenly distributed spheroids with the same invasion pattern along radially aligned fibers. (B) Multiphoton second-harmonic generation images of T47D tumor spheroids after a 10-day invasion show no collagen fiber orientation changes. Confocal images of (C) T47D and (D) MCF7 tumor spheroids after a 10-day invasion exhibit multicellular disseminated clusters

and finger-like projections invading along radially aligned fibers with a magnified inset for multicellular disseminated cell clusters. **(E)** MCF7 and **(F)** T47D tumor spheroids in the Couette + gravity group display more complicated borders than random and gravity only groups. **(E-F)** Box and whisker plot with mean and 95% CI (n=20 spheroids per group from three independent experiments). **** $p < 0.0001$ by one-way ANOVA.

Author Manuscript

Author Manuscript

Author Manuscript

Author Manuscript

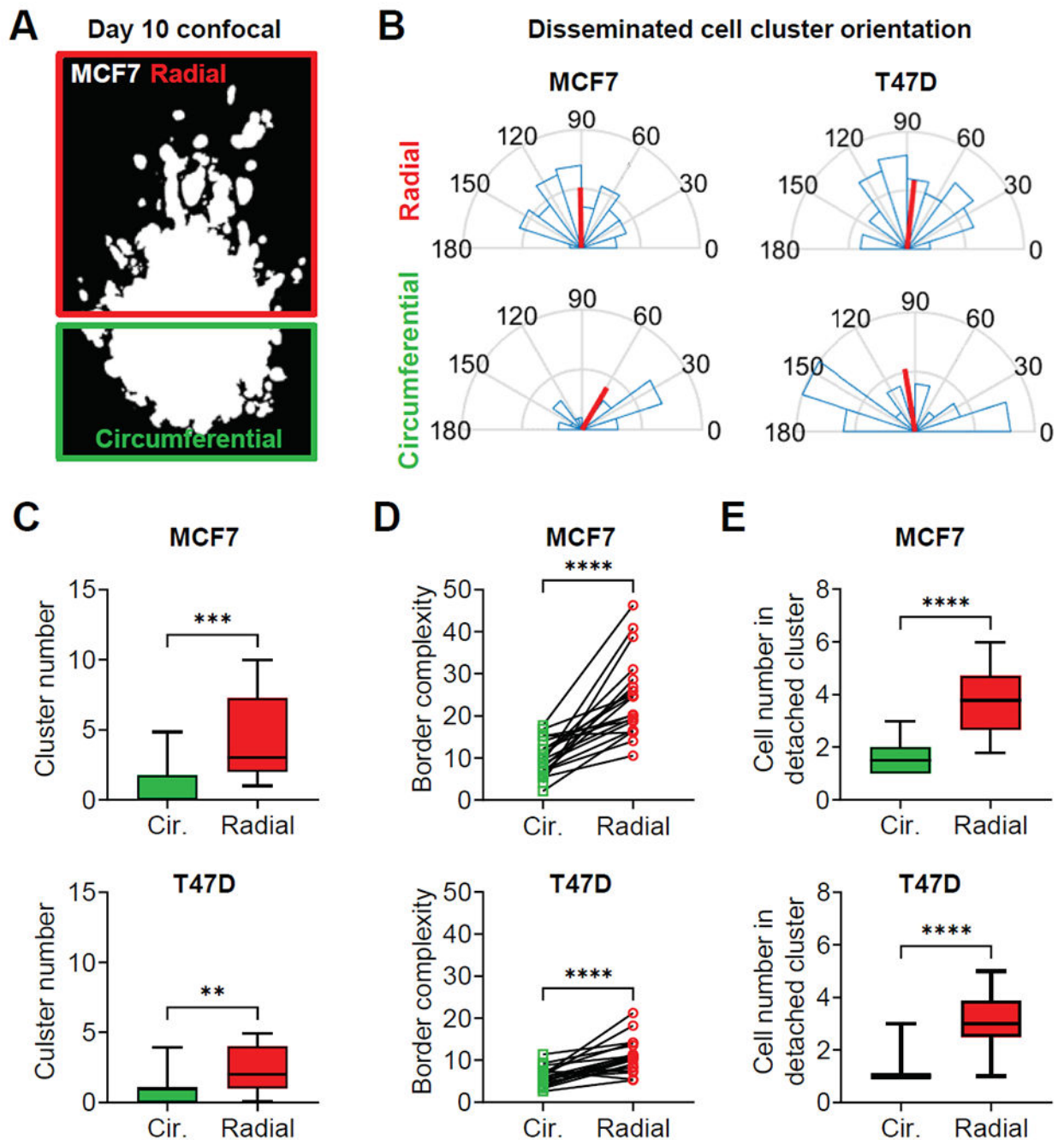


Figure 6. Radially aligned fiber topography promotes cell cluster-based collective cancer invasion.

(A) A binary image of an MCF7 tumor spheroid after a 10-day invasion. (B) Disseminated cell clusters invade along the direction of radially aligned or circumferentially oriented fibers. Red lines represent the magnitude and direction of mean resultant vectors. (C) More clusters of cells are disseminated from main tumors on the radial zone than circumferential zone. ** $p < 0.01$, *** $p < 0.001$ by Student's t-test. (D) Border complexities are greater on the radial zone than circumferential zone. **** $p < 0.0001$ by Wilcoxon matched-pairs

signed-rank test. **(E)** Cell numbers of the disseminated cell clusters are higher on the radial zone than circumferential zone. * $p < 0.05$, *** $p < 0.001$ by Student's t-test. **(C and E)** Box and whisker plot with mean and 95% CI **(C-E)** $n=20$ spheroids per group from three independent experiments.

Author Manuscript

Author Manuscript

Author Manuscript

Author Manuscript

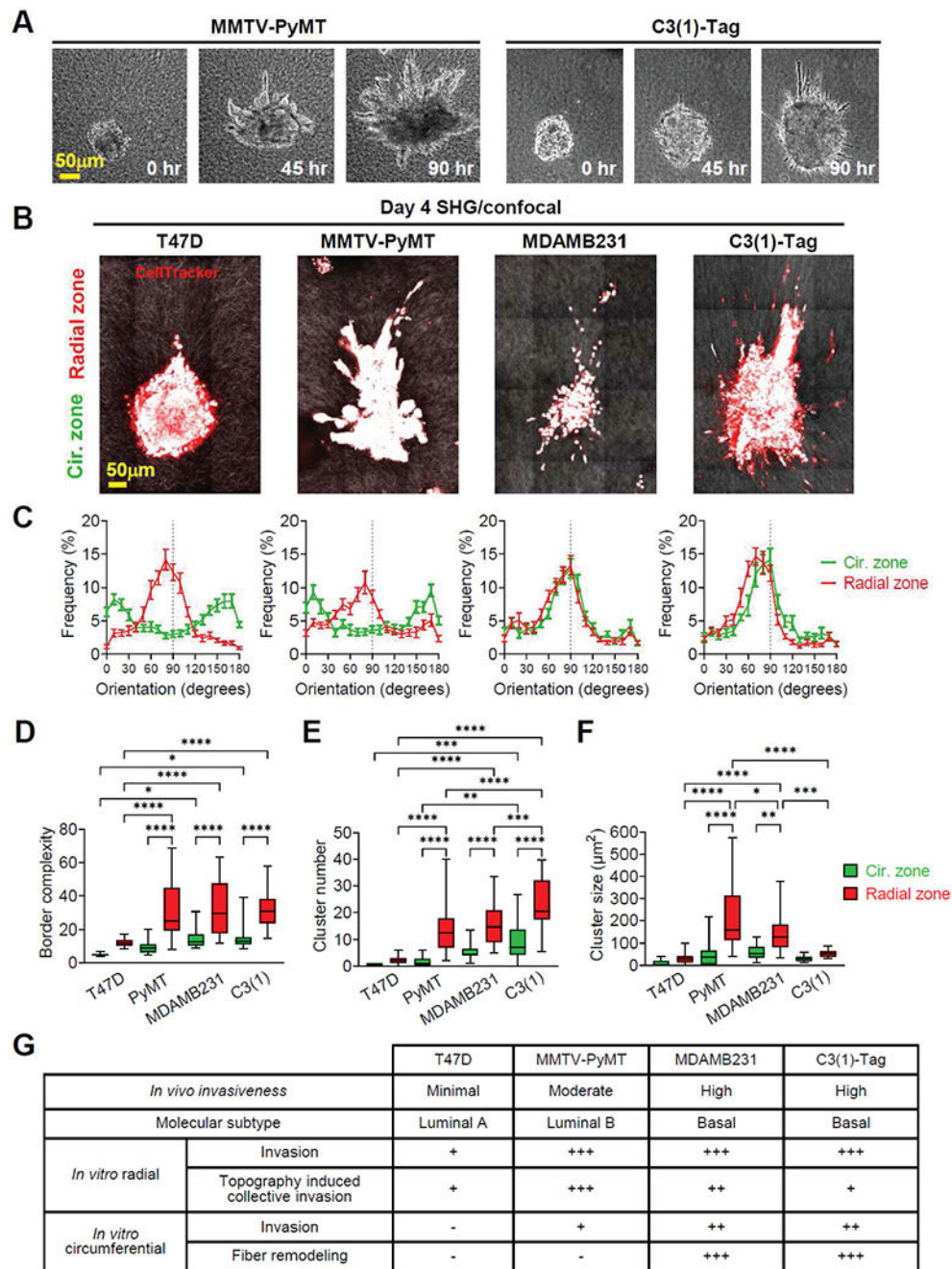


Figure 7. Dual topographical tumor model distinguishes tumor spheroids and organoids invasion pattern.

(A) Time-lapse images of MMTV-PyMT and C3(1)-Tag mouse mammary tumor organoids in dual topographical tumor models. (B) Multiphoton second-harmonic generation and confocal images of T47D and MDAMB231 human breast tumor spheroids and MMTV-PyMT and C3(1)-Tag mouse mammary tumor organoids after a 4-day invasion. (C) The fiber orientation frequency distribution of originally radial and circumferential zones after a 4-day invasion indicates fiber orientation remodeling by MDAMB231 spheroids and

C3(1)-Tag organoids but neither by T47D spheroids nor MMTV-PyMT organoids. Data are mean \pm SEM (n=20 spheroids or organoids per group from three independent experiments). **(D)** Border complexity, **(E)** disseminated cell cluster number, and **(F)** disseminated cell cluster size of tumor spheroids/organoids. **(G)** *In vivo* invasiveness, molecular subtypes, and *in vitro* invasion pattern in dual topographical model of tumor spheroids/organoids. **(D-F)** Box and whisker plot with mean and 95% CI (n=20 spheroids/organoids per group from three independent experiments). * $p < 0.05$, ** $p < 0.01$, *** $p < 0.001$, **** $p < 0.0001$ by one-way ANOVA.

Table 1.

Previous tumor models with the predisposed ECM structure

Techniques to pre-align ECM fibers	Cell models	Findings	Limitations	References
Multicellular spheroid				
Cellular contraction of adjacent cell spheroids	MDA-MB-231 spheroids seeded in microcavities	Cell spheroids apply tensile force to align ECM fibers which in turn guide collective migration	Microcavities used to embed spheroids may interrupt the predisposed ECM structure Fiber alignment in restricted areas	[34]
Single cell				
Cellular contraction of fibroblasts followed by decellularization	MDA-MB-231 individual cell-laden hydrogel attached to pre-aligned collagen gel	Aligned fibers enhance the directional migration of cancer stem cells	Cancer cell-laden hydrogel was attached adjacent to but not seeded within pre-aligned fibers Decellularization may damage the predisposed collagen fiber structure	[18, 19]
Confined geometry and vacuum flow guidance in microfluidics	MDA-MB-231 individual cell pre-seeded in collagen gel before alignment	Cancer cells migration in aligned fibers is Rho-independent		[9]
Injection force into hydrogel interface	MDA-MB-231 and MCF7 individual cells pre-seeded in collagen gel before alignment	Aligned fibers enhance cancer cell intravasation	Challenging to be applied as a tumor spheroid model because pre-seeded tumor spheroids may interfere with the alignment methods	[20]
Microfluidics-driven shear flow	MDA-MB-231 and HCT-116 individual cells pre-seeded in collagen gel before alignment	Microscale collagen bundles enhance cancer cell migration		[21]
Needle rotation strain aligns fibers after collagen gelling	MDA-MB-231 and MTLn3 individual cell pre-seeded in collagen gel	Cancer cells migration directionality in aligned fibers is ROCK dependent	Nonhomogeneous directionality of fiber alignment	[61, 62]
Electrospinning	Cancer cells or tumor spheroids seeded onto electrospun scaffolds	Aligned fibers enhanced cancer cell migration	Difficult to embed tumor spheroids in high-density electrospun fibers	[35, 82, 83]